Pharmacological Research 175 (2022) 105996

Contents lists available at ScienceDirect

Pharmacological Research

journal homepage: www.elsevier.com/locate/yphrs

iTReX: Interactive exploration of mono- and combination therapy dose response profiling data

Dina ElHarouni [a,b,c,d], Yannick Berker [b,e], Heike Peterziel [b,e], Apurva Gopisetty [b,c], Laura Turunen [f], Sina Kreth [b,g], Sabine A. Stainczyk [b,g], Ina Oehme [b,e], Vilja Pietiäinen [f], Natalie Jäger [b,c], Olaf Witt [b,e,h], Matthias Schlesner [a,i,1], Sina Oppermann [b,e,*,1]

[a] Bioinformatics and Omics Data Analytics, German Cancer Research Center (DKFZ), Heidelberg, Germany
[b] Hopp Children's Cancer Center (KiTZ), Heidelberg, Germany
[c] Division of Pediatric Neurooncology, German Cancer Research Center (DKFZ) and German Cancer Consortium (DKTK), Heidelberg, Germany
[d] Faculty of Biosciences, Heidelberg University, Heidelberg, Germany
[e] Clinical Cooperation Unit Pediatric Oncology, German Cancer Research Center (DKFZ) and German Cancer Consortium (DKTK), Heidelberg, Germany
[f] Institute for Molecular Medicine Finland (FIMM), Helsinki Institute of Life Science (HiLIFE), University of Helsinki, Helsinki, Finland
[g] Division of Neuroblastoma Genomics, German Cancer Research Center (DKFZ) and German Cancer Consortium (DKTK), Heidelberg, Germany
[h] Department of Pediatric Oncology, Hematology, Immunology and Pulmonology Heidelberg University Hospital, Heidelberg, Germany
[i] Biomedical Informatics, Data Mining and Data Analytics, Faculty of Applied Computer Science and Medical Faculty, University of Augsburg, Augsburg, Germany

ARTICLE INFO

Keywords:
Therapy response profiling and exploration
Interactive drug screen analysis
Asymmetric sensitivity scoring
Differential combination sensitivity scoring
Personalized medicine
Drug target networks

ABSTRACT

High throughput screening methods, measuring the sensitivity and resistance of tumor cells to drug treatments have been rapidly evolving. Not only do these screens allow correlating response profiles to tumor genomic features for developing novel predictors of treatment response, but they can also add evidence for therapy decision making in precision oncology. Recent analysis methods developed for either assessing single agents or combination drug efficacies enable quantification of dose-response curves with restricted symmetric fit settings. Here, we introduce iTReX, a user-friendly and interactive Shiny/R application, for both the analysis of mono- and combination therapy responses. The application features an extended version of the drug sensitivity score (DSS) based on the integral of an advanced five-parameter dose-response curve model and a differential DSS for combination therapy profiling. Additionally, iTReX includes modules that visualize drug target interaction networks and support the detection of matches between top therapy hits and the sample omics features to enable the identification of druggable targets and biomarkers. iTReX enables the analysis of various quantitative drug or therapy response readouts (e.g. luminescence, fluorescence microscopy) and multiple treatment strategies (drug treatments, radiation). Using iTReX we validate a cost-effective drug combination screening approach and reveal the application's ability to identify potential sample-specific biomarkers based on drug target interaction networks.

The iTReX web application is accessible at https://itrex.kitz-heidelberg.de

1. Background

Functional cell-based therapy profiling approaches have become crucial in both basic biomedical research and in preclinical studies, and play an important role in establishing novel anti-tumor therapeutic strategies in precision medicine [1–3]. Quantitative assessment of therapy efficacy using cell models is mostly based on dose responses profiled at multiple concentrations in multi (96-, 384-, or 1536-) well plates. Cells are screened against a library of drugs or treatments (e.g., fractionated radiation therapy) to determine the relative sensitivity and resistance of cells to each treatment. Viability or death of treated cells can be measured using various readouts such as luminescence (e.g., CellTiter-Glo® assay), absorbance (e.g., MTT assays) [4], or fluorescence (e.g., flow cytometry, fluorescence microscopy) [5], either on a well-based or on a single cell level. The standard analysis of such drug profiling data usually includes quality control, readout normalization, dose-response curve fitting, as well as drug hit ranking based on a

* Corresponding authors at: Clinical Cooperation Unit Pediatric Oncology, German Cancer Research Center (DKFZ) and German Cancer Consortium (DKTK), Heidelberg, Germany
[1] Authors share last authorship.

https://doi.org/10.1016/j.phrs.2021.105996
Received 10 September 2021; Received in revised form 18 November 2021; Accepted 19 November 2021
Available online 27 November 2021
1043-6618/© 2021 The Authors. Published by Elsevier Ltd. This is an open access article under the CC BY-NC-ND license (http://creativecommons.org/licenses/by-nc-nd/4.0/).

Nomenclature

4PL	4-Parameter Logistic
5PL	5-Parameter Logistic
AA	Activity Area
absIC25	absolute Inhibitory Concentration 25
absIC50	absolute Inhibitory Concentration 50
Amin	minimum activity threshold
ATP	Adenosine Triphosphate
AUC	Area Under the Curve
BRAFV600E	proto-oncogene B-Raf
BzCl	Benzethonium Chloride
CDKN2A	Cyclin Dependent Kinase Inhibitor 2A
cellHTS	cell High Throughput Screening
CNN	Convolutional Neural Network
COMPASS	Clinical implementation Of Multidimensional PhenotypicAl drug SenSitivities in pediatric precision oncology
CRA-mod	Combination therapy Response Analysis module
CTG	CellTiter-Glo
CVD	Coefficient of Variability in Difference
dcDSS_asym	differential combination asymmetric Drug Sensitivity Score
DIP	Drug-Induced Proliferation
DMSO	Dimethyl Sulfoxide
dPI	differential Percentage Inhibition
DSS	Drug Sensitivity Score
DSS_asym	asymmetric Drug Sensitivity Score
DSS_asym,adjusted	adjusted asymmetric DSS
Emax	Maximum Effect reached
ETV6-NTRK3	ETS Variant Transcription Factor 6 - Neurotrophic Receptor Tyrosine Kinase 3
FBS	Fetal Bovine Serum
FIMM	Institute for Molecular Medicine Finland
gCSI	Genentech Cell Line Screening Initiative
GDSC	Genomics of Drug Sensitivity in Cancer
GOF	Goodness Of Fit
GR	Growth Rate
GRAY	Oregon Health and Science University Breast Cancer Screen by Dr Joe Gray's lab
GUI	Graphical User Interface
HSA	Highest Single Agent
HitNet-mod	drug Hits interaction Network mapping module
IC50	Inhibitory Concentration 50
Imax	maximum possible attainable percent inhibition
Imin	minimum possible attainable percent inhibition
IMT	Inflammatory Myofibroblastic Tumor
INDELs	insertions and deletions
INFORM	INdividualized Therapy FOr Relapsed Malignancies in Childhood
iTReX	interactive Therapy Response eXploration
MRA-mod	Monotherapy Response Analysis module
MTT	3-(4,5-dimethylthiazol-2-yl)-2,5-diphenyltetrazolium bromide
nplr	n-parameter logistic regression
NDR	Normalized Drug Response
NEAA	Non-Essential Amino Acid
OTP	One Touch Pipeline
PBMCs	Peripheral Blood Mononuclear Cells
PDC	Patient-Derived Cell Culture
PDX	Patient-Derived Xenograft
QCN-mod	Quality Control and Normalization module
R^2	coefficient of determination
relIC50	relative Inhibitory Concentration 50
sDSS_asym	selective asymmetric DSS
SNVs	Single Nucleotide Variants
STS	Staurosporine
TPM	Transcripts Per Million
TRK	Tyrosine Kinase

consensus of sensitivity thresholds [2].

Reproducibility of quantitative cell-based therapy response profiling remains a challenge due to variability in experimental and computational settings [6]. One of the most challenging computational aspects is the drug response curve fitting, for which different models exist. The four-parameter logistic (4PL) model has been widely used to fit the relation between doses and responses in pharmacological experiments, assuming that the vast majority of therapy responses would follow a symmetric sigmoid curve [7–10]. Alternative model functions derived from the logistic model include the generalized five-parameter logistic (5PL) model, which results in an asymmetric dose-response curve and may better represent the therapy response curve behavior [11]. Hence, multiple state-of-the-art R packages for dose-response curve fitting and analysis include both 4PL and 5PL models [12,13]. The final model performance is estimated using weighted or non-weighted goodness of fit, which can be used to select the model of choice for each curve [13]. Moreover, constraint settings of the fitted curve such as assuming a minimum inhibition of 0% and a maximum of 100% affect the goodness of fit and force curves to deviate from the readings that represent cell proliferation [14].

Curve fitting acts as a basis for assessing single pharmacokinetic parameters or metrics depending on multiple parameters [15,16] including approaches combining the slope, area under the curve (AUC) and the maximum effect reached (Emax) [2,15,17]. Moreover, the fitted curve parameters provide the basis for computing the concentration at which 50% of the maximum response is reached (IC50), which represents a measure of potency of the therapy. In addition, Emax represents the efficacy of the treatment [18]. Since single model parameters can capture only limited information about the differences in the response patterns, the AUC is used as a metric combining both potency and efficacy, yet it suffers from similar limitations as IC50 and Emax measurements [15]. Hence, further computational developments have been implemented aiming to integrate the multi-parametric values into a single score, such as the drug sensitivity score (DSS) [19]. Although the DSS proposed by Yadav et al. shows a better performance in comparison to the IC50, AUC and the area over the dose-response curve (activity area-AA) metric [18], it is still implemented for up to 4PL models, and it is often used with constraint curve fitting [19].

Therapeutic agents are routinely combined to achieve therapeutic benefits in various medical fields, specifically in clinical oncology [20]. Systematic drug combination testing across cell lines, patient-derived xenografts (PDX), or patient-derived cell cultures (PDCs), including organoids, presents the opportunity to discover novel drug combinations [21]. Synergy and antagonism of therapy combinations are often quantified by the comparison of an experimentally obtained effect and the mathematical reference effect of a null-reference model [22]. Several experimental and computational methods are available to identify synergism in combination screens (synergy matrix screens) [23], in which a range of dose responses with all dose pairs of two combination agents within the chosen concentration ranges are tested. However, the limiting factor for efficient usage of synergy matrix screens for patient -derived material is often the high number of cells required for testing of several drug combinations simultaneously. Thus, a minimal-input combination experimental setup has been used to tackle

the limitations on the sample material, which consists of the addition of a single fixed concentration of a combination drug (or treatment) to a drug library tested over a concentration range [24]. In comparison to other matrix-based combination approaches testing all possible combinations of two concentration ranges (i.e., 4 × 4, 6 × 6, 8 × 8), this minimal-input combination can be written as a 2 × N matrix for each drug combination (library drug and combination drug). Thus, each matrix consists of two rows, representing a single-agent (library drug alone) and a combination screen (library drug plus fixed concentration of the combination drug), respectively, and N columns, representing a full concentration range of the library therapy drug. In the presented screens, a combination drug is used at a single non-zero concentration (solvent only, conc = 0, and fixed concentration, conc > 0) and a range of 5 concentrations is used for a library drug, presenting a 2 × 5 matrix screen.

While preclinical studies often rely on drug combination screening, only few of the recently described quantitative sensitivity metrics have been adjusted to include the DSS metric in the evaluation of combination screens. To date, there are several openly available analysis tools for analyzing monotherapy drug screening data, such as cellHTS [25], PharmacoGx [26], GRmetric [27], and Breeze [28]. Moreover, analysis methods [29] and platforms have been developed for synergy matrix screens [30–32]. However, most of these analysis platforms are restricted to 4PL models and all of them are limited to the analysis of either single agent screens or synergy screens and none of the platforms enable the visualization of drug target networks nor map omics data to the hit drug targets reported to identify potential biomarkers.

To address the above-mentioned challenges, we developed the **i**nteractive **T**herapy **R**esponse **eX**ploration (iTReX) application for the analysis of both mono- and combination therapy response profiling data with an unconstraint dose-response fitting method. We use an extended DSS with 5PL scoring, including an asymmetric DSS curve fitting and integration method. For analysis of combinatorial treatment response, iTReX further provides a computational method to calculate differential combination Drug Sensitivity Scores ($dcDSS_{asym}$) values from various treatments strategies for capturing synergies for experiments with limited material and reduced experimental costs. iTReX is available as a web-based Shiny application (https://itrex.kitz-heidelberg.de), enabling users to analyze raw values of therapy response profiling screens with various modalities (i.e., luminescence, absorbance, fluorescence) or preprocessed screen output data (e.g., cell viability/death). The workflow allows users to easily process datasets from small-, medium- to high-throughput therapy screens and provides a basis for interpretation of the treatment response data by calculating and visualizing quality control outputs, drug sensitivity metrics, and interaction network maps. Therapy hits are visualized in several formats such as heatmaps and waterfall plots on a sample or cohort basis. The therapy hit outcomes can be used to construct drug targets interaction networks and/or mapped to omics features of the processed sample to explore potential biomarkers. iTReX aims to support users from the field of therapy discovery, preclinical and clinical research, therapy decision making and the translation of *ex vivo* results into the clinic. Analysis examples within this study are shown from the field of pediatric precision oncology, however, iTReX can also be used for any other disease areas aiming to identify therapy efficacies and potential drug repurposing opportunities.

2. Materials and methods

2.1. Implementation

iTReX (v1.1.0) is developed as a Shiny application. Its modules use state of the art R packages, in addition to extended and newly developed functionalities. General data visualization, data manipulation, and report generation utilize public R libraries (ggpubr [33], dplyr [34], stringr [35], rmarkdown [36]). All presented results have been obtained with iTReX v1.1.0.The QCN-mod assesses the screen quality control and performs therapy response normalization. The MRA-mod uses the nplr package [13] for dose-response fitting using the residuals weight method and an extended version of the DSS [2]. The DSS was extended from a 4-parameter integral scoring model [19] to a 5-parameter integral in order to consider the asymmetry coefficient (Asym) along with the 4PL parameters including the x-coordinate at the inflection point (Xmid), Hill slope (Slope), the bottom and top asymptotes (Rmin and Rmax) respectively and the activity threshold (Amin).

$$DSS_{asym} \propto \int_{R \geq Amin} R\_asym(x)dx = I(Xmid, \quad Slope, \quad Rmin, \quad Rmax, \quad Amin, \quad \boldsymbol{Asym})$$

The selective DSS is computed by subtracting the asymmetric DSS of healthy (reference) samples from the asymmetric DSS of the tumor (subject) sample [28], with each drug being tested in the same concentration range for the tumor (subject) sample and healthy (reference) samples. The computed score is used to distinguish subject selective from general toxic therapeutics. The higher the $sDSS_{asym,}$ the more selective is the therapy for the tumor (subject) sample. A $sDSS_{asym}$ close to zero indicates a non-selective therapy while a negative $sDSS_{asym}$ would indicate therapeutics with a higher effect in the healthy (reference) samples compared to the tumor (subject) sample.

$$sDSS_{asym} = DSS_{asym}\ (tumor) - DSS_{asym}\ (healthy)$$

The adjusted DSS_{asym} and the adjusted $sDSS_{asym}$ represent a fine-tuned DSS_{asym} and $sDSS_{asym}$, respectively, using the goodness of fit (GOF), where the GOF is computed using the nplr package [13].

$$DSS_{asym,adj} = GOF * DSS_{asym}$$

$$sDSS_{asym,adj} = DSS_{asym,adj}\ (tumor) - DSS_{asym,adj}\ (healthy)$$

The CRA-mod computes the differential combination DSS metric ($dcDSS_{asym}$) via a comparative analysis between the combination and monotherapy DSS metrics, in which the DSS_{asym} (combo) is calculated for a treatment tested in 5 concentrations in combination with a therapy tested at a fixed concentration. DSS_{asym} (mono) refers to the monotherapy sensitivity of the same treatment tested in 5 concentrations solely without the addition of the combination treatment fixed dose. Normalization of the raw values is performed separately for both the mono- and combination therapy, where the screening negative controls (e.g., DMSO) of the combo therapy must include the fixed combined treatment. The $dcDSS_{asym}$ aims to estimate the enhanced effect of a combination treatment within one score.

$$dcDSS_{asym} = DSS_{asym}\ (combo) - DSS_{asym}\ (mono)$$

In order to explore the antagonistic, synergistic or enhanced effects of a combination treatment on a per dose basis, the CRA-mod computes a matrix of differential Percentage Inhibition (dPI) over therapies (t) and doses (d), where PI represents the inhibition fitted values.

$$dPI^{(t,\ d)} = PI^{(t,\ d)}\ (combo) - PI^{(t,\ d)}\ (mono)$$

The HitNet-mod is implemented to construct drug perturbation connectivity maps for the top n drugs that are defined by the user. An annotation table of drug names to their respective drug target genes must be uploaded by the user as an input. The top n selected targets are then used to construct the interaction network using OmniPathR, where the interactions are retrieved from the SignaLink database [37], and visualized using igraph [38].

The Omics-mod uses the molecular features of the specific analyzed sample, uploaded and provided by the user, to visualize matched events of the omics file to the HitNet-mod constructed map, allowing the visualization of multiple molecular events occurring within the interaction network.

2.2. Validation datasets

2.2.1. Pharmacogenomic datasets analysis

We used the MRA-mod to analyze raw viability drug response data of the GDSC (v2–8.0) [39], FIMM (v2016) [40], gCSI (v2017) [41], and GRAY (v2013) [42] datasets. The goodness of fit was used to assess the performance of the n logistic parameter fitting among all datasets. See the "Data availability" section for raw drug sensitivity data access.

2.2.2. CRA-mod analysis of combination synergy screen by O'Neil et al. 2016

The O'Neil et al. dataset was used to validate the efficiency of the CRA-mod. Monotherapy raw data was first adjusted to span the same concentration ranges as the combination therapy raw data provided. The DSS_{asym} scores were computed for all monotherapies, and drugs with a calculated $DSS_{asym} > 10$ were selected as *hits* and further included in the CRA-mod analysis. The DSS_{asym} cutoff of 10 was selected based on the performance of the symmetric DSS score described by Yadav et al., where drug sensitivity was observed for DSS scores starting in a range of (10−15) in a set of acute myeloid leukemia *ex vivo* screen [19]. Moreover, the same cutoff was selected by Malani et al., where glucocorticoids showed an enhanced sensitivity in AML samples exceeding an *ex vivo* drug sensitivity score threshold of 10 [43]. Of note, a hit identification threshold can depend on the sensitivity of an individual sample and may vary based on entity and screening setup. For the CRA-mod analysis, only one concentration (closest to the absolute IC25) for each of these hits was selected as the concentration for the combination partner to be added on top of the whole drug library, here as a theoretical approach for analysis only. The selected combinations were analyzed using the MRA-mod and the DSS_{asym} scores were recorded. The CRA-mod finally was used to compute the $dcDSS_{asym}$ as the difference between DSS_{asym} of the drug combination to its respective monotherapy. The differential percentage inhibition (dPI) was computed for each combination concentration. For the validation of the reproducibility of the results the median $dcDSS_{asym}$ across the screened cell lines was calculated for each drug and compared to the median Bliss scores for synergistic effects and the median Highest Single Agency (HSA) score for quantifying antagonism. The Bliss score is a synergy metric that compares the observed effect of a drug combination to the expected effect based on the assumption that the two drugs act independently [44]; the HSA score represents the maximum single drug effect [29,45]. Both scores were retrieved from the DrugComb portal [32] for the full synergy matrix. See the "Data availability" section for data access.

2.3. Established human cell lines and PDX screening

2.3.1. Cell culture

Demonstration of the monotherapy analysis using iTReX was conducted using two human cancer cell lines, BT-40 and INF_R_153. The BT-40 low grade glioma cell line harboring a BRAF V600E mutation and CDKN2A deletion was provided by Peter J. Houghton (UT Health, San Antonio, Texas) and is described by Bid et al. [46]. The INF_R_153 cell line was generated from a primary tumor biopsy obtained from an inflammatory myofibroblastic tumor (IMT) enrolled in the INFORM registry study by the CWS study group (Prof. Ewa Koscielniak, Klinikum Stuttgart, Germany). Presence of the ETV6-NTRK3 fusion was confirmed by RNA-Seq analysis. Details of the INFORM study including Ethics Commitee approval and patient consent is described by Pfaff et al. [47].

The BT-40 and INF_R_153 cells were cultured in RPMI 1640 containing L-glutamine (Gibco, Life Technologies) supplemented with 10% fetal bovine serum (FBS) and 1x non-essential amino acid solution (NEAA). Cell lines were expanded to 70% confluency before drug screening.

The healthy (reference) sample repository consisted of five samples (one human fetal astrocyte (HA-1800 cell line) and 4 primary peripheral blood mononuclear cells samples (PBMCs)). The PBMC samples were collected from enrolled pediatric and young adult patients (age < 21) enrolled in the INFORM registry study and were submitted by the respective GPOH study centers for functional drug testing within 24 h after surgery. PBMCs were purified from heparin blood after two-fold dilution in RPMI using Ficoll Paque Premium (17–5446–52, GE Healthcare). PBMC samples underwent drug screening without preculturing and were seeded at a concentration of a minimum 5000 cells/well onto the pre-dispensed drug plates.

The INF_R_1632 PDX model was established from a fresh surgical specimen of an INFORM patient with relapsed neuroblastoma by subcutaneous engraftment of cells isolated from a fresh surgical specimen into immune-compromised mice. One tumor-bearing mouse was sacrificed when the volume of the subcutaneous PDX tumor reached 500 mm^3. The mouse was anesthetized using 1.5–2.5 vol% isoflurane.

The harvested tumor tissue (260 mg) was minced thoroughly with sterile scissors and further processed according to a protocol adapted from Stewart et al. [48]. Briefly, the mechanically homogenized tissue was enzymatically dissociated by incubating with 1.2 μg/ml trypsin (T9935, Sigma-Aldrich) in Neurobasal-A medium (10888022; Life Technologies) for ~30 min at 37 °C in a water bath. Digestion was stopped by adding 1.2 μg/ml trypsin inhibitor (T6522, Sigma-Aldrich), followed by repeated addition of 60 μl 1 mg/ml DNase in 0.5 M $MgCl_2$ until settlement of the remaining tumor fragments to the bottom of the tube was observed. The cell isolate was passed through a 40 μm cell strainer (352340; Corning) and spun down at 800 rpm for 5 min at room temperature. Red blood cells were removed by resuspending the cell pellet in 2 ml ACK Lysing buffer (LONZ10–548E; Lonza), incubating for 2 min at room temperature and washing with TSM base medium [Supplementary Table 1]. Subsequently, the cells were seeded at a density of 3 × 106 cells per ml in TSM complete medium [Supplementary Table 2]. The cells formed free-floating three-dimensional spheroids and semi-adherent spheroids.

Three days after tumor dissociation, the media containing free-floating spheroids were collected and centrifuged at 500 g for 5 min. Subsequently, the spheroids were dissociated by using 1 ml TrypLE Express (12604013; Life Technologies) and incubation at 37 °C for 5 min. The semi-adherent cells were detached with 1 ml TrypLE Express at 37 ° for 5 min from the cell culture dish. The dissociated cells were combined in 5 ml TSM base, spun down at 500 g for 10 min at room temperature, and resuspended with TSM complete medium [Supplementary Table 1] for cell counting. Drug screening was performed using 1000 cells/well (4×10^4 cells/ml) in TSM complete medium in U-shaped round-bottom 384-well plates (3830; Corning) as described below.

2.3.2. Drug response testing

A customized drug library consisting of 76 oncology drugs [Supplementary Table 3] was dispensed with an Echo 550 acoustic dispenser (Labcyte) to three round-bottom 384-well microplates (ready-to-go assay plates) by the High Throughput Biomedicine core unit (FIMM, HiLIFE, University of Helsinki, Finland). Each drug was transferred in five different concentrations, each as duplicate/plate, covering a 10,000-fold concentration range. 0.1% DMSO and 100 μM BzCl were used as negative and positive controls in 25 μl final volume. The empty wells were included in all drug screening plates for 1) media only, no cells, and 2) for cells only, no treatment as previously described [16]. These *ready-to-go assay* plates were shipped to the local laboratory and stored in storage pods at RT under nitrogen gas until further use. For therapy response testing, cells were seeded on top of the pre-dispensed drugs in 25 μl of respective media per well at a density of 500 cells/-well (2×10^4 cells/ml), 1000 cells/well (4×10^4 cells/ml) or 5000 cells/well (2×10^5 cells/ml) as described above. Seeding of cells in U-shaped 384-well round bottom plates allowed for formation of three-dimensional spheroid cultures as one spheroid/well, ideally. Cells were incubated at 37 °C and 5% CO_2 for 72 h, and the cell viability was measured as ATP-based cell viability with CellTiter-Glo® Luminescent Cell Viability Assay (CTG, G9243, Promega), using a FLUOstar OPTIMA

reader (BMG LABTECH) or TECAN SPARK plate reader with top optic and 1 s integration time. Additionally, cells were imaged using nuclear Hoechst (H3570, Thermo Fisher Scientific) staining in a no wash protocol and 30 min incubation followed by fluorescent microscopy using the ImageXpress Micro Confocal (Molecular Devices, San Jose, CA) high-content microscope.

2.3.3. Combotherapy response testing

The drug combination screen (INF_R_1632_V1_PDX_CS1, referred to in the following as INF_R_1632) for the PDX derived cells included the addition of a fixed concentration of 10 nM Trametinib, dispensed on top of the *ready-to-go assay* plates using a Tecan D300 drug printer on top of one replicate of each concentration of the 76 compound library described above. Trametinib was identified as one of the top hit drugs (most effective and clinically relevant) from a previously conducted single agent screen as described above using the same model and output of the MRA-mod analysis. The concentration of 10 nM represents the nearest administered concentration to the absolute IC25 as a single agent activity of Trametinib in the PDX model. All 76 drugs were tested as single agents and in combination with Trametinib within the same plate allowing for computation of the differential combination asymmetric DSS ($dcDSS_{asym}$). For replicate measurements, identical copies of each assay plate were measured. Otherwise, the screening was performed as described above.

2.3.4. Omics data

2.3.4.1. WES and WGS data processing. Whole-exome (WE) and Whole-genome sequencing (WGS) was performed for the BT-40 and INF_R_153 cell lines. Sequencing reads were aligned by the DKFZ One Touch Pipeline (OTP) [49] against the human reference genome (version GRCh37d5) [49]. The SNV and INDEL calling workflows are based on samtools/bcftools with additional custom filters (optimized for somatic variant calling by deactivating the pval-threshold in bcftools) and Platypus 0.8.1, respectively [50,51] as previously described [52]. The standard SNV and INDEL calling workflow was extended with filters developed for samples without matched control (no control workflow). HUGO gene nomenclature symbols of the called coding mutations were used as an input for the iTReX application.

2.3.4.2. RNAseq data processing. RNA sequencing data for the BT-40 and INF_R_153 cell lines were processed by the DKFZ OTP pipeline [49]. Transcripts Per Million (TPM) values were scaled for each cell line, and z-scores greater than 0.5 were identified as highly expressed genes per sample.

2.3.4.3. Identification of fusion genes. Fusion genes from the RNA-seq data were identified using Arriba v2.1.0. (Arriba: Fast and accurate gene fusion detection from RNA-seq data) [53], available at https://github.com/suhrig/arriba)

Molecular features for BT-40 and INF_R_153 are provided in [Supplementary Table 11 and 14], respectively.

3. Results

3.1. Overview of iTReX

iTReX was implemented within the Shiny framework (https://shiny.rstudio.com/), combining the computational versatility of R with a user-friendly and interactive web interface. It integrates state of the art medium to high throughput screening analysis approaches [2,13] with further extended and newly developed mono- and combination therapy response metrics. The application provides quantitative analysis for the therapy response data, hit scoring, and visualization of functional therapy results. In addition, it can be used to construct a sample specific drug-targets interaction network and map omics features to the network. Thereby, iTReX offers a complete workflow through five main functional modules: (i) the Quality Control and Normalization module (QCN-mod), (ii) the Monotherapy Response Analysis module (MRA-mod), (iii) the Combination therapy Response Analysis module (CRA-mod), (iv) the potential drug Hits interaction Network mapping module (HitNet-mod), and (v) a module for identifying potential sample-specific omics-based biomarkers from the drug target connectivity networks (Omics-mod). Results of quantitative outputs from the MRA and CRA modules can be visualized per individual sample or per cohort, consisting of multiple samples. An overview heatmap can be constructed to allow the comparison of therapy responses across samples (cohort analysis) with multiple clustering distance methods.

Any numerical data, obtained by various techniques, including luminescence counts of ATP-based viability measures (CTG; CellTiter-Glow) or e.g., cell- or well based outputs from microscopic imaging data, can be utilized, either as raw value or as normalized inhibition data. iTReX accepts a tabulated file as input [Supplementary Table 4], holding the coordinates for each well in the multi-well plate, a therapy name and the tested concentration, allowing for customized plate layouts, and raw or normalized read measurements. An example data file can be downloaded within the iTReX application for multiple formats of viability readouts demonstrating mono- or combination therapies performed on a single sample or a full cohort. Moreover, a demonstration of a pre-processed imaging-based readout is available [Supplementary Table 5], where the imaging numerical measurements were computed using an image- analysis approach utilizing convolutional neural networks (CNNs) [54]. The layout used in the imaging screen can also be uploaded separately as exemplified in [Supplementary Table 6] where Staurosporine is annotated as an image-specific positive control at a fixed concentration of 250 nM and further used as treatment control (TRC) in a concentration series in this demonstration screen. The user can specify the type of readout uploaded (cell viability or cell death) according to the type of measurement used in the screen; cell death settings were selected for the demonstrated imaging data. Finally, iTReX supports the generation of interactive HTML visualization reports and tabulated spreadsheets, which can be downloaded from the output of the complete workflow [Fig. 1]. A user manual is provided within the home page of the iTReX application to support the user with step-by-step instructions. The user manual includes detailed information about data preparation, setting screening parameters, uploading data and results exploration. It further includes layout and data file demonstration examples allowing the user to test the application without the need of own data.

3.2. Quality control and normalization module (QCN-mod)

In order to detect potential technical errors in the raw data of therapy response profiling and to determine the quality of the analyzed screen as a first critical step in the data analysis workflow, iTReX includes the QCN-mod as an initial step to asses and visualize the quality of the screen(s) before further processing modules. A quantitative quality control summary table [Supplementary Table 7] is computed by the QCN module to assess discrepancies between screened wells (Sample/Control) across one or multiple plates. The summary table includes Z' metrics to show the separation between the distributions of the positive and negative controls. According to [25], an ideal Z' would be 1, an excellent assay would have a Z' between 0.5 and 1, a marginal assay would lie between 0 and 0.5, and an overlap between positive and negative controls would result in a negative Z'. The QCN module computes the Z' using the coefficient of variability in difference (CVD), and the robust CVD that is less sensitive to outliers by using the median and the mean absolute deviation [55]. The quality control summary table includes the mean, standard deviation, and the coefficient of variation for each measured well type (i.e., positive control, negative control). Furthermore, the module normalizes raw read counts to the provided controls. In case both positive and negative controls are provided, the

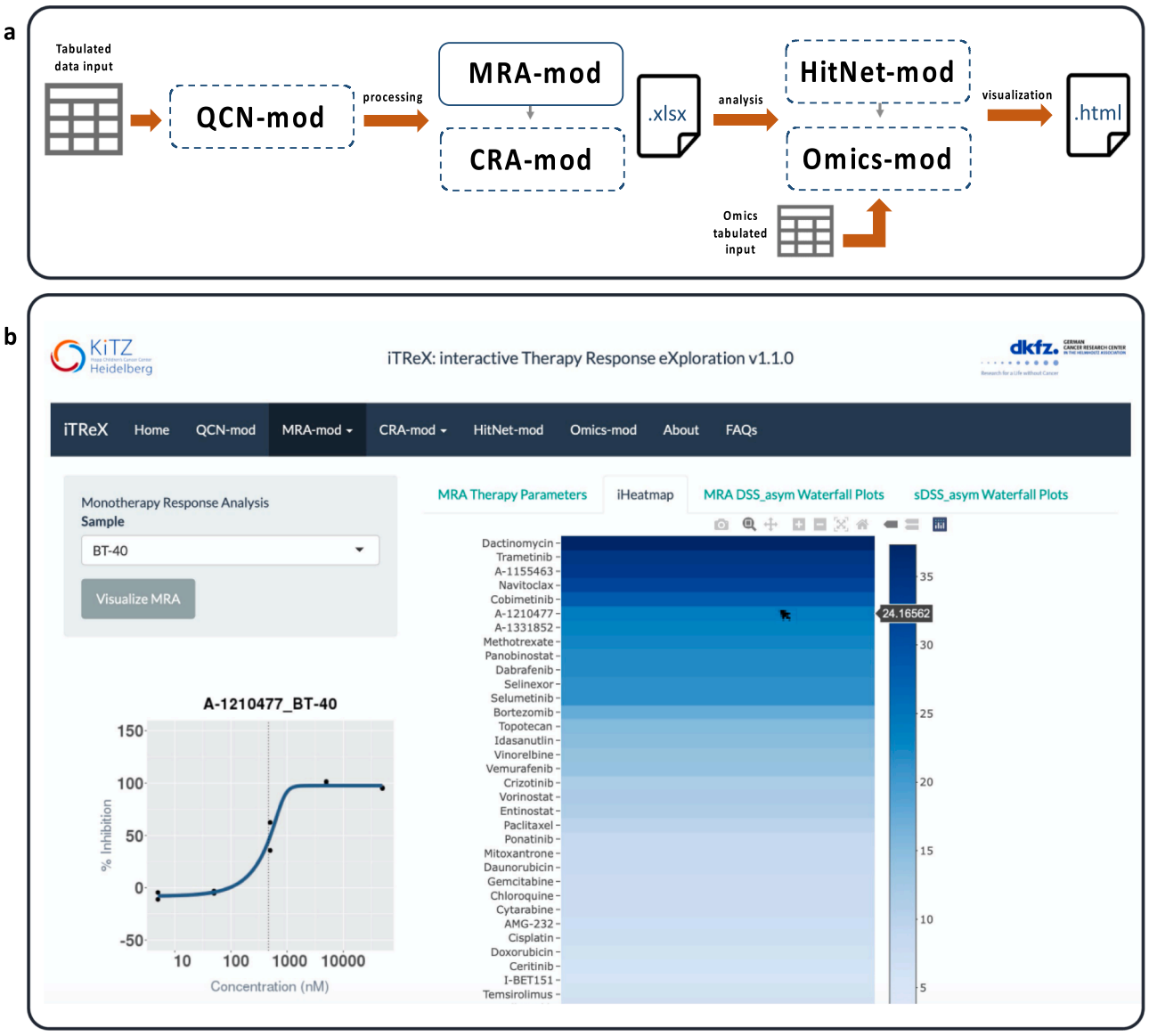

Fig. 1. A schematic overview of the iTReX application. (a) Overview of iTReX analysis workflow, where tabulated therapy plate layouts and/or screen readouts are accepted as input. Analysis can be performed using five analysis and visualization modules. **(b)** iTReX web interface from the MRA module output, where the user can explore therapy parameters, or visualize an interactive heatmap of asymmetric drug sensitivity score (DSS_{asym}) ordered descending with a gradient blue color scheme. In addition, the user can hover interactively over the heatmap to visualize the fitted dose-response curves for each therapy, where the gray area surrounding the curve line indicates the standard error based on the goodness of fit. The MRA module includes further tab panels to visualize waterfall plots representing the DSS_{asym} score and the selective DSS_{asym}, which reveals selective vs. non-selective toxic therapies in case one or more healthy (reference) samples were uploaded.

module performs the normalization of drug responses, which was shown to improve the accuracy and consistency of quantification of anti-cancer drug sensitivity [17].

The QCN module output includes the visualization of plate raw count distribution [Fig. 2a], plate layouts [Fig. 2b] and raw counts per well type box plots to detect variability between the screened plates and wells [Fig. 2c]. Often, therapy response profiling measures are performed in replicates to control reproducibility and to increase the precision of results. The QCN module calculates and visualizes the correlation between replicates and computes the Pearson correlation coefficient [Fig. 2d]. Furthermore, the measures (e.g., viability) of positive and negative controls are shown in a masked well-based heatmap to visually detect possible control outliers and technical errors that may occur in positive and negative control wells [Fig. 2e]. The outputted plots aid in identifying outlier wells visually. This allows the user for instance to manually exclude those wells from the raw data and re-upload the sample(s) to iTReX. Z-transformed and raw viability heatmaps are also generated for all uploaded plates to visualize possible edge effects [Fig. 2f]: it is nonetheless recommended to fill the outer rows and columns of a multi-well plate with either just media ("empty" wells) and/or untreated cells in media ("untreated" wells) as demonstrated in this study [Fig. 2b], [Fig. 2f] to decrease evaporation effects which mostly occur in outer wells of a multi well plate format. A layout example of the plate design including empty and untreated wells used for this study is provided within the iTReX application for download and presented in [Supplementary Table 4]. A therapy control response (TRC) curve can also be included to verify the positive control drug behavior post data normalization. The therapy control serves as validation for the assay performed, where the visualization of the therapy response curve [Fig. 2g] allows the user to check the expected behavior and determine technical faults visually that can be observed. Gray bands are plotted above and below fitted curves to indicate the goodness of the model fit, which is computed using the coefficient of determination R^2 between the measured and predicted inhibition values. Bands are $+ -100 * (1 - R^2)$

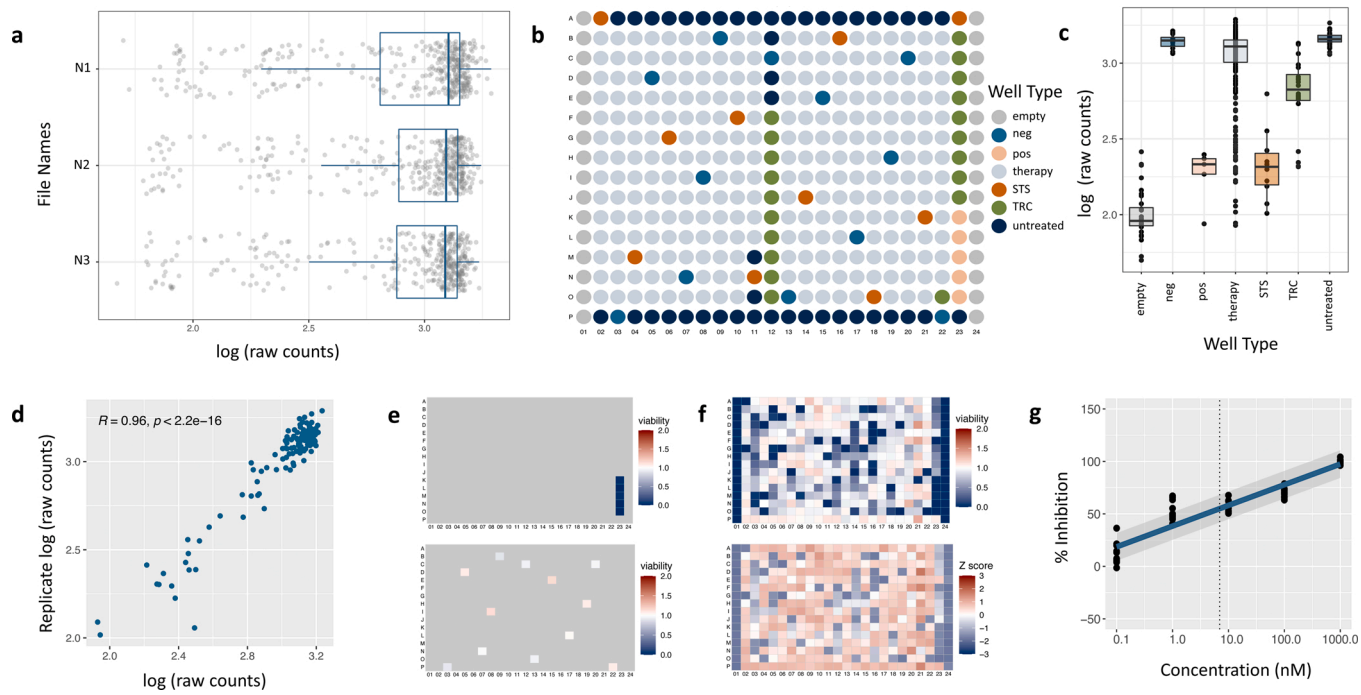

Fig. 2. Overview of Quality Control and Normalization module output. A demo QCN output based on a drug sensitivity profiling of a BT-40 cell line using the ATP-based cell viability readout (CTG). **(a)** Raw measurement distribution, representing log10(raw counts) per screened plate. **(b)** Plate layout distribution of empty wells (with no cells), negative control wells (Dimethyl sulfoxide - DMSO), positive control wells (Benzethonium Chloride - BzCl), sample (tested therapies), therapy control wells (TRC; Staurosporine), and untreated wells (cells in culture media only). **(c)** log10(raw count) distribution per well type per plate. **(d)** Correlation plot of replicate screens. **(e)** Raw viability plot for positive (upper panel) and negative (lower panel) controls distributed per plate, where the positive controls show low viability raw counts (blue), and the negative controls show a higher viability (white – light red). **(f)** Z-transformed and raw viability plate heatmaps with a divergent color scale between low viability values (blue) and high viability values (red). **(g)** Therapy control response curve. STS was measured as quadruplicates for five concentrations per plate (n = 3). Gray area above and below the curve indicates the goodness of the model fit as statistical measure.

units wide along the vertical direction, so they have a width of ±100 for the worst-possible fit while being invisible for perfectly fitting models. Finally, a report can be downloaded in HTML format.

3.3. *Monotherapy response analysis module (MRA-mod) considers asymmetry in therapy response metric scoring*

The MRA-mod was developed to analyze monotherapy responses. The module starts with fitting the dose-response curve of each drug or therapy based on the normalized inhibition values using a weighted ("residual weights", to reduce the effect of possible outliers) n-parameter logistic model integrated in the log-concentration domain using the nplr R package [13], where n is an integer ranging between 2 and 5. A 5PL model fits the dose-response curves based on the top and bottom asymptotes, Hill coefficient, the inflection point, and the asymmetry coefficient. The 2PL model depends only on the Hill coefficient and the inflection point, while assuming that the bottom and top asymptotes are strictly constraint to 0% and 100%, respectively, and a constant asymmetric coefficient of 1. The 3PL model further optimizes the top asymptote over the 2PL, while the 4PL model also optimizes the bottom asymptote [Supplementary Fig. 1]. The module then computes minimum and maximum attainable percent inhibition values (Imin, Imax) from the bottom and top asymptotes, capped at − 10% and 110%, respectively. Furthermore, the module computes the relative inhibitory concentration (relIC50) at which the inhibition is halfway between minimum and maximum attainable inhibition, the absolute 25%- and 50%-inhibitory concentration (e.g., absIC25 – concentration at which 25% inhibition is reached), an asymmetric drug sensitivity score based on the unconstraint 5PL curve model (DSS_{asym}), and a selective asymmetric DSS ($sDSS_{asym}$) in case the measurements for a control sample or a healthy (reference) samples are provided. The computed metrics and a dose-response curve for each fitted therapy can be downloaded as a spreadsheet [Supplementary Table 8]. Therapy top hits can be visualized as a waterfall plot interactively using either metric (DSS_{asym} or $sDSS_{asym}$). Additionally, the MRA-mod uses the coefficient of determination (R^2) between the fitted and the observed inhibition values as a goodness of fit (GOF) measure for each therapy and re-ranks therapies using the adjusted DSS_{asym} ($DSS_{asym,adj}$) and $sDSS_{asym,adj}$ values [Supplementary Fig. 2]. The user can select the number of top hits to be included and download the plots as an HTML report. Interactive heatmaps can be explored in a sample-specific manner or visualized as comparative heatmaps for a cohort of multiple samples.

The 5PL model considers the asymmetric coefficient during fitting, which is assumed to be equal to one in the state-of-the-art 4PL model. Thus, it is expected that the 5PL yields a better or at least as good GOF as the 4PL fitting model, since the set of 5PL models is a strict superset of 4PL models. To validate whether nplr detects the asymmetric advantage, we reanalyzed available pharmacogenomic datasets. Raw measurements for drug response profiles were recovered from (i) the Genomics of Drug Sensitivity in Cancer (GDSC) [39] dataset, comprising 1109 cell lines tested against 250 drugs; (ii) the Institute for Molecular Medicine Finland (FIMM) compound testing assay [40], covering 52 drugs across 50 cancer cell lines; (iii) the Genentech Cell Line Screening Initiative (gCSI) [41], profiling 754 cell lines and 16 drugs; and iv) the Oregon Health and Science University Breast Cancer Screen by Dr Joe Gray's lab (GRAY) [42], spanning 84 breast cancer cell lines tested against 90 drugs. Among all the reanalyzed datasets, the asymmetric 5th parameter sigmoidal fit was most often the best performing fitting method according to the GOF for the drug dose responses tested [Fig. 3a]. Although nplr may return another model than 5-PL as the best fitting model due to independent initialization of all candidate models, nplr was able to detect the advantage of the 5PL model in two thirds of the curves, while yielding the most commonly used 4PL result in another 25% of curves. [Fig. 3b] shows that nplr couldn't capture the advantage

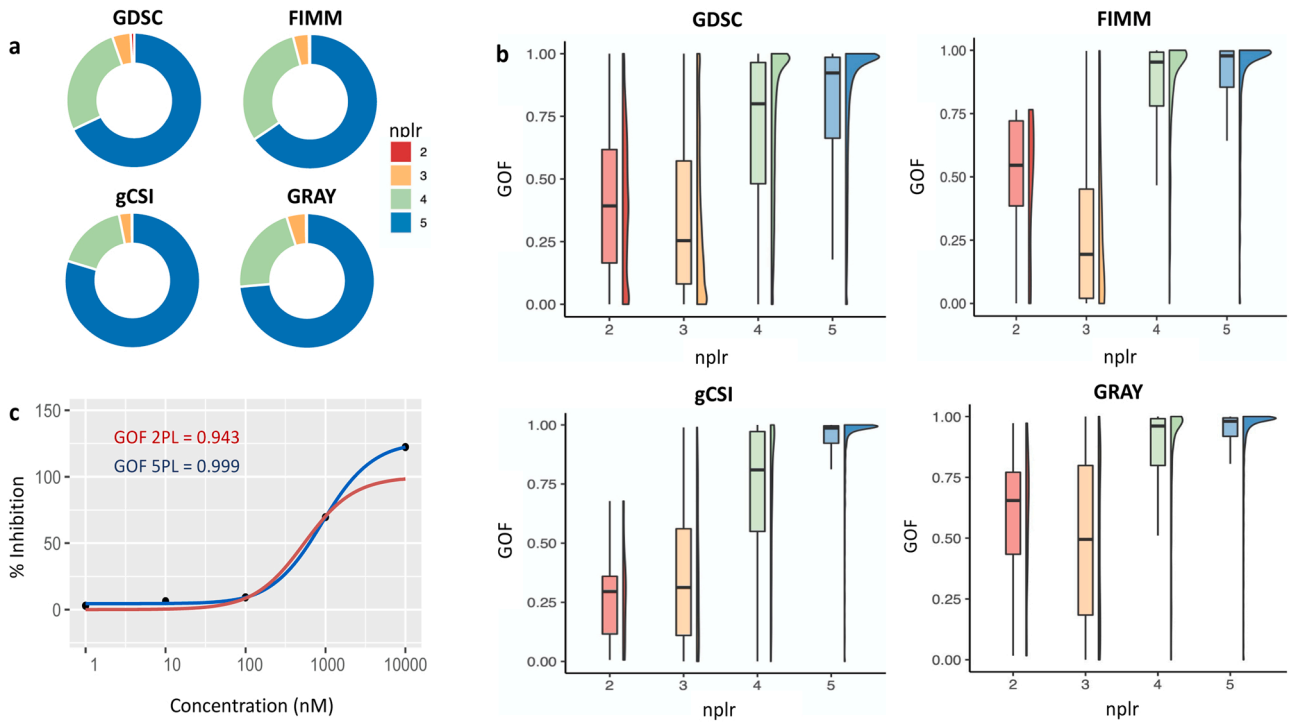

Fig. 3. Weighted n-parameter dose-response fitting performance across pharmacogenomic datasets. (a) Pie charts illustrating the ratio of the selected best performing logistic model based on the goodness of fit. **(b)** Adjacent box and half violin plots showing the goodness of fit distribution among the selected best performing fitting parameter across different datasets. **(c)** Difference between the constraint fit 2PL method (red) and the 5PL (blue) curve fitting.

in one third of the curves because either 4PL models could be fit with a high GOF (dose-response curves for which a 4PL model can be fit without detriment), or 2PL/3PL models were the best fit but still had a low GOF, indicating curves of bad quality, which can be excluded by down-weighting using the $DSS_{asym,adj}$ metric available in the MRA-mod. [Fig. 3c] demonstrates in one representative example the difference in curve fitting and the GOF between the 2PL and 5PL models.

3.4. Combination therapy response analysis module (CRA-mod) detects combination synergy hits in a cost-effective approach

iTReX includes a module to analyze combination screens, which can be based on a monotherapy library screen and a combination library screen, in which a specific treatment is added at a single concentration on top of the concentration range of the full drug library. These minimal-input combination screens were previously described by Lanevski et al. as a cost-effective experimental design with DECREASE tool [56]. Moreover, a similar combination screen was conducted by Oppermann et al. [24], where the experimental aim was to detect the maximum combination enhancements of a 380 kinase inhibitor library in combination with a specific inhibitor chosen at a fixed concentration, hence one fixed concentration of a drug (Venetoclax at 10 nM) was added to each of the drugs included in the full kinase inhibitors library. Such an experimental setting can be of advantage in case of limited patient-derived material and may be used as an exploratory analysis for preliminary hit identification of synergistic combination therapies. This could be achieved by combining a single concentration of one or more monotherapy top hit(s) to a library of therapy options, tested in several concentrations. However, the use of multi-parametric quantitative sensitivity metrics, such as the DSS, were not implemented previously to detect synergy and antagonism in combination settings. Hence, the CRA-mod was introduced within iTReX to aid the computational analysis of the minimal-input combination screens. iTReX can analyze combinations of different therapy types, such as drug-drug and or drug-radiation based profiling. The CRA-mod compares the DSS_{asym} of the combined therapeutic agent to the respective tested monotherapy in an asymmetric differential combination drug sensitivity score ($dcDSS_{asym}$) and visualizes dose response curves of both, combination and monotherapy in one plot to indicate possible synergistic (left), additive (middle) and antagonistic effects (right) [Fig. 4a, b]. Furthermore, a matrix of differential Percentage Inhibition (dPI) values per applied dose can be calculated and visualized in a heatmap view to identify top hit therapies per dose, thus allowing the classification of potentially antagonistic ($dPI < 0$), additive ($dPI = 0$) or potentially synergistic ($dPI > 0$) effects per dose. Differential percentage inhibition is shown as example for the drugs that showed an enhanced effect according to the dcDSS metric ($dcDSS_{asym} > 0$) in [Fig. 4d]. CRA-mod analysis output can be downloaded as a spreadsheet including the detailed calculation outputs [Supplementary Table 9]. We demonstrate the functionalities of the CRA-mod using a combination drug screening on cells derived from a neuroblastoma PDX model INF_R_1632. The model was developed from a tumor biopsy sample of a neuroblastoma patient enrolled in the INdividualized Therapy FOr Relapsed Malignancies in Childhood (INFORM) registry study [57]. Here, Trametinib was combined at a concentration of 10 nM with a drug library of 76 compounds tested at five concentrations per drug [Supplementary Fig. 3]. The module output is shown in [Fig. 4]. Nilotinib was detected as the most efficient drug in combination with Trametinib, indicated by a $dcDSS_{asym}$ of 6.22, followed by Mitoxantrone, Navitoclax, Venetoclax and Cisplatin as the top 5 hits for combination therapy based on the $dcDSS_{asym}$ [Fig. 4b]. The synergistic effect between Nilotinib and MEK inhibitors has been also previously reported by several tumor models [58–60]. [Fig. 4c] demonstrates the synergistic effect of Trametinib (10 nM) and Nilotinib in the INF_R_1632 combination screen. Furthermore, the screen identifies the combination of Volasertib (PLK1 inhibitor) and Trametinib as additive, indicated by an overlap of both dose response curves for mono- and combination therapy [Supplementary Fig. 4], and dPI values around zero for each of the tested concentrations and a $dcDSS_{asym}$ near zero (-

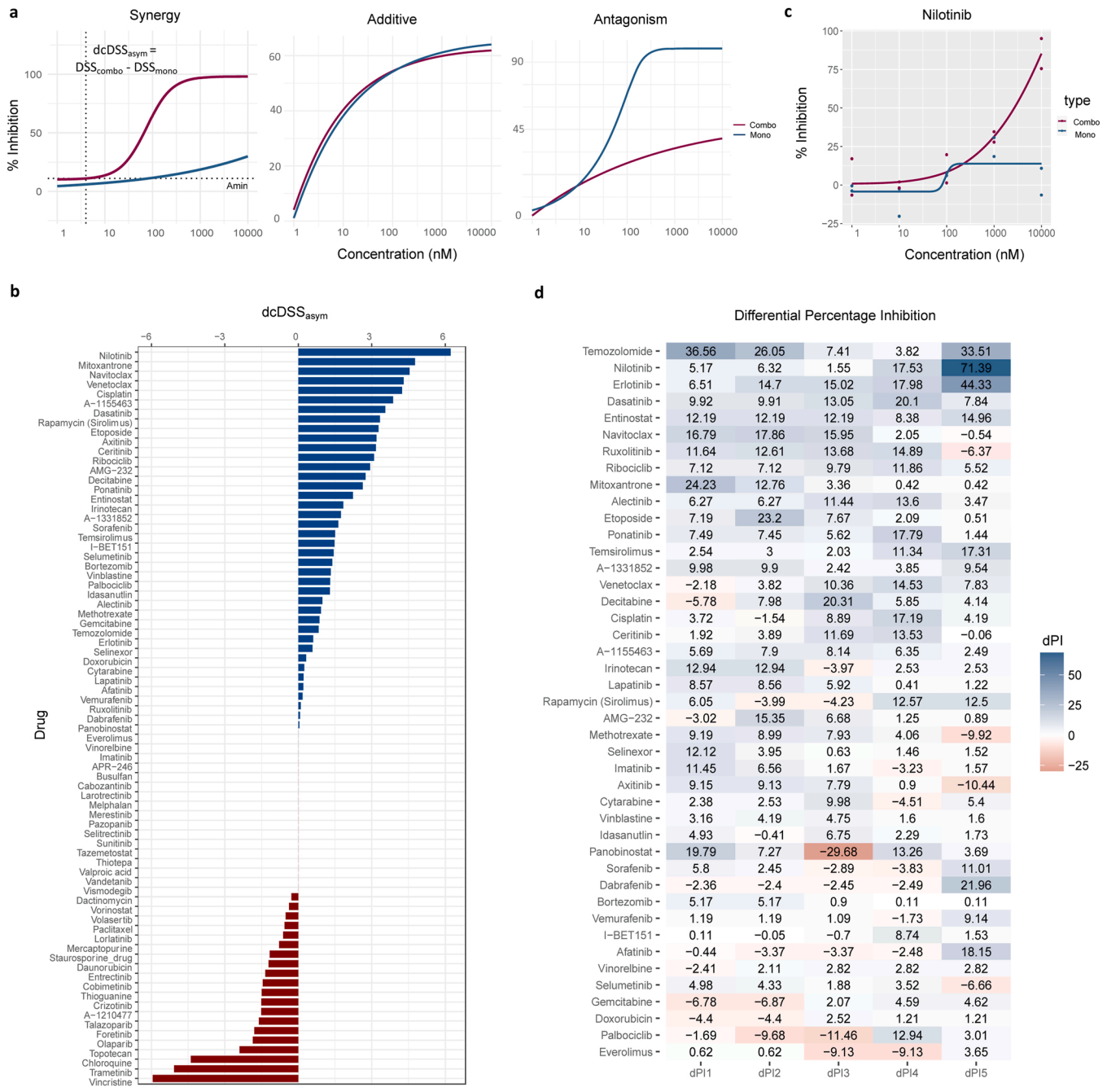

	dPI1	dPI2	dPI3	dPI4	dPI5
Temozolomide	36.56	26.05	7.41	3.82	33.51
Nilotinib	5.17	6.32	1.55	17.53	71.39
Erlotinib	6.51	14.7	15.02	17.98	44.33
Dasatinib	9.92	9.91	13.05	20.1	7.84
Entinostat	12.19	12.19	12.19	8.38	14.96
Navitoclax	16.79	17.86	15.95	2.05	−0.54
Ruxolitinib	11.64	12.61	13.68	14.89	−6.37
Ribociclib	7.12	7.12	9.79	11.86	5.52
Mitoxantrone	24.23	12.76	3.36	0.42	0.42
Alectinib	6.27	6.27	11.44	13.6	3.47
Etoposide	7.19	23.2	7.67	2.09	0.51
Ponatinib	7.49	7.45	5.62	17.79	1.44
Temsirolimus	2.54	3	2.03	11.34	17.31
A−1331852	9.98	9.9	2.42	3.85	9.54
Venetoclax	−2.18	3.82	10.36	14.53	7.83
Decitabine	−5.78	7.98	20.31	5.85	4.14
Cisplatin	3.72	−1.54	8.89	17.19	4.19
Ceritinib	1.92	3.89	11.69	13.53	−0.06
A−1155463	5.69	7.9	8.14	6.35	2.49
Irinotecan	12.94	12.94	−3.97	2.53	2.53
Lapatinib	8.57	8.56	5.92	0.41	1.22
Rapamycin (Sirolimus)	6.05	−3.99	−4.23	12.57	12.5
AMG−232	−3.02	15.35	6.68	1.25	0.89
Methotrexate	9.19	8.99	7.93	4.06	−9.92
Selinexor	12.12	3.95	0.63	1.46	1.52
Imatinib	11.45	6.56	1.67	−3.23	1.57
Axitinib	9.15	9.13	7.79	0.9	−10.44
Cytarabine	2.38	2.53	9.98	−4.51	5.4
Vinblastine	3.16	4.19	4.75	1.6	1.6
Idasanutlin	4.93	−0.41	6.75	2.29	1.73
Panobinostat	19.79	7.27	−29.68	13.26	3.69
Sorafenib	5.8	2.45	−2.89	−3.83	11.01
Dabrafenib	−2.36	−2.4	−2.45	−2.49	21.96
Bortezomib	5.17	5.17	0.9	0.11	0.11
Vemurafenib	1.19	1.19	1.09	−1.73	9.14
I−BET151	0.11	−0.05	−0.7	8.74	1.53
Afatinib	−0.44	−3.37	−3.37	−2.48	18.15
Vinorelbine	−2.41	2.11	2.82	2.82	2.82
Selumetinib	4.98	4.33	1.88	3.52	−6.66
Gemcitabine	−6.78	−6.87	2.07	4.59	4.62
Doxorubicin	−4.4	−4.4	2.52	1.21	1.21
Palbociclib	−1.69	−9.68	−11.46	12.94	3.01
Everolimus	0.62	0.62	−9.13	−9.13	3.65

Fig. 4. CRA-mod analysis and visualization outputs. A combination therapy response analysis screen of cells derived from a neuroblastoma PDX model (INF_R_1632). Trametinib (IC25 ~ 10 nM) was combined with the full concentration range of a 76 drug library. **(a)** The differential combination drug sensitivity score (dcDSS$_{asym}$) calculation as mathematical demonstration of possible combination scenarios, reflecting the area between the monotherapy and the combination therapy dose-response curve after achieving the minimum activity threshold (Amin). The Amin is 10% of the maximum achievable inhibition. The plot represents a mathematical demonstration of the expected output of a synergistic combination effect, where the combination therapy DSS$_{asym}$ exceeds the DSS$_{asym}$ value of the monotherapy (left), an expected additive effect (middle), and the antagonistic effect (right). **(b)** Waterfall plot representing the dcDSS$_{asym}$ score calculated to compare combination and monotherapies, where the blue bars indicate a positive enhanced effect of the combination therapy (i.e., a positive dcDSS$_{asym}$). The red bars indicate an combination effect with a negative dcDSS$_{asym}$. The additive effect of Trametinib in combination with other drugs with a dcDSS$_{asym}$ score of zero are aligned between the enhanced and the antagonistic agents bar plots. **(c)** Synergistic dose-response curves of Nilotinib-Trametinib combination therapy (deep-pink) and Nilotinib monotherapy (blue) from the CRA analysis output of INF_R_1632 PDX model. **(d)** Matrix plot of top hit therapy combinations representing the differential percentage inhibition (dPI) of each drug (five concentrations along matrix rows) in difference between the combination and monotherapy percentage inhibition.

0.51). Notably, in case of additive effects both dose response curves aid to be overlapping due to the normalization procedure of single agent versus combination therapy separately to their respective controls. The potential for combining MEK inhibitors (i.e., Trametinib) with PLK1 inhibitors (Volasertib) was previously reported for malignant melanomas and melanoma cell lines, supporting a correlation between MEK and PLK1 signaling [61–63].

To validate the performance of the CRA-mod algorithm in detecting

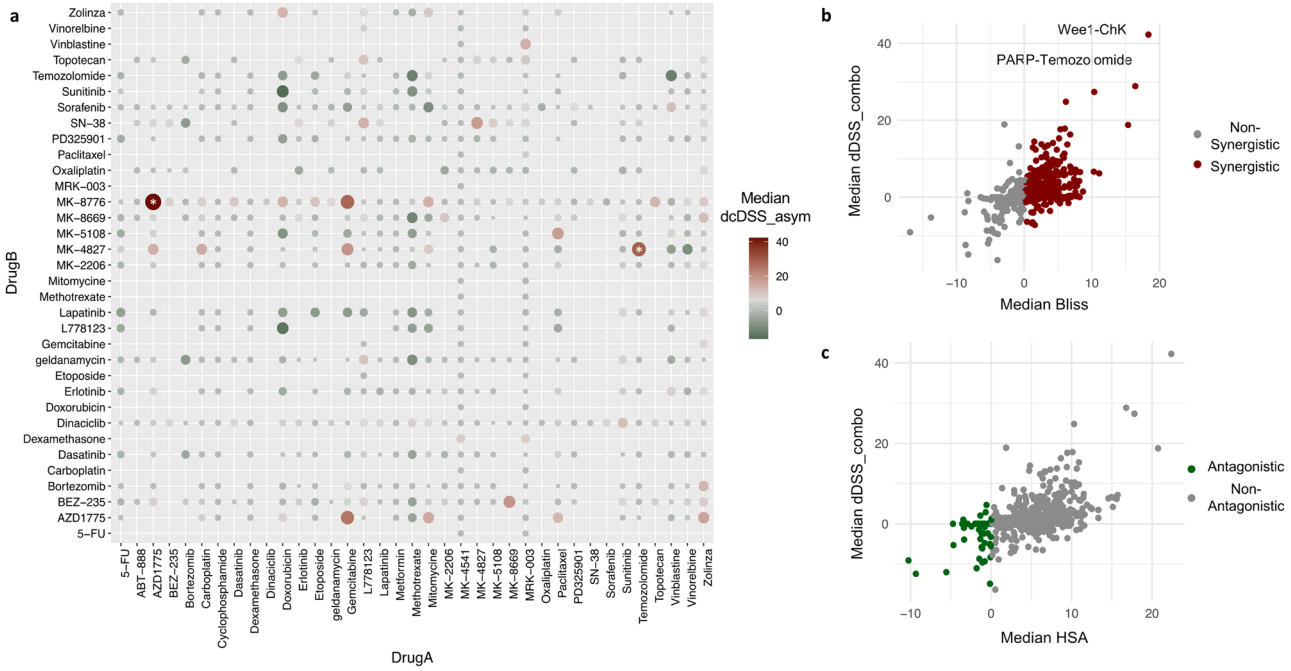

Fig. 5. Reproducibility of CRA-mod using the Merck combination synergy screen dataset. (a) The Merck dataset CRA-mod output, in red is the enhanced effect drug combinations, while the antagonist effect is indicated in green. The top two enhanced combination effects are labeled with asterisks (MK8776-AZD1775) and (MK4827-Temozolomide). The red divergent scale represents the synergistic median value of the $dcDSS_{asym}$, while the green color divergent scale represents the antagonistic values of the median $dcDSS_{asym}$ metric. Both color intensity and dot size reflect the absolute magnitude of the median of the measured score ($dcDSS_{asym}$). **(b)** Reproducibility of the Merck dataset synergistic results, comparing median Bliss independent synergy scores to the median $dcDSS_{asym}$ scores. Bliss scores higher than 0.12 indicate synergistic effects, while combinations shown in gray are considered non-synergistic. **(c)** Reproducibility of the Merck dataset antagonistic results, comparing median HSA scores to the median $dcDSS_{asym}$ scores. HSA scores below 0.12 (green) indicate antagonism.

synergism with a reduced cost-effective experimental approach we used HT drug combination screening data published by O'Neil et al. [64]. This dataset includes 22,737 experiments for 583 drug combinations tested on 39 cancer cell lines using a 4 × 4 dosing regimen, where Bliss scores above 0.12 were considered synergistic combinations and the Highest Single Agent (HSA) scores less than 0.12 were considered antagonistic [32]. The CRA-mod was able to reproduce the results [Fig. 5] reported by O'Neil et al. using the minimal-input combination analysis method. The minimal-input was achieved by combining a single concentration nearest to IC25 of monotherapy hits, which showed a DSS_{asym} above 10 to the full concentration ranges of the monotherapy library computed by the MRA-mod. Using the minimal-input approach we were able to reduce the O'Neil et al. dataset to include 9652 experiments among 551 combinations in the CRA-mod analysis. Using the iTReX CRA-mod, we identified top combination hits, which were in line with the reported synergies among the tested cell lines [64]. The reproduced top enhanced combination effects included the Wee1 inhibitor (AZD1775), in combination with the ChK1 inhibitor (MK8776), and the PARP inhibitor (MK4827) in combination with Temozolomide. The Wee1-ChK1 synergy has also been confirmed in an *ex vivo* screening study of acute myeloid leukemia [65], and explained by synergistic DNA damage during the S-phase by Hauge et al. [66]. The PARP inhibitors have shown synergistic effects in combination with Temozolomide in vitro and in vivo [67], in addition to a synergistic effect of the later combination therapy in a PDX co-clinical trial on relapsed small-cell lung cancers [68] and Ewing's sarcoma cells [69]. Thus, the CRA-mod is able to analyze minimal-input combination screens and captures possible combination treatment similar to the large effort matrix screen. We conclude that this approach could be used as a first screening approach allowing to test multiple combinations in a primary setting with the need of less sample material and drug amount to identify potential combination hits, which can then be further validated in larger preclinical synergy screens.

3.5. HitNet-mod and Omics-mod detect matches between top therapy hits and molecular profiles of ex vivo PDCs and identify potential druggable biomarkers using drug target interaction network mapping

Prior knowledge networks of interactions and roles of proteins in intra- and intercellular signal transduction, as well as transcriptional and post-transcriptional regulation, can give biological insights into the mechanisms of drug target interactions. To provide a comprehensive view of selected drug hits, iTReX enables users to explore the interactions between top hit drugs and their targets.

To enable a network-based overview of drug target interactions and the visual exploration of signaling pathways, cross-talks and multi-pathway proteins we have used the HitNet-mod by visualizing top hit drug target genes interactions using pathway information from Omni-Path [37]. Furthermore, the Omics-mod can be used to map the molecular profile on the drug targets interaction network of the sample. To this end, the user can upload a tabulated file with HUGO gene symbols of the molecular events per sample (e.g., gene fusions, single nucleotide variants, and insertions and deletions).

To demonstrate the use of HitNet and Omics-mod within the application, we provide examples of ATP-based cell viability screens of two pediatric cancer cell models, where we were able to match the drug target information with relevant molecular aberrations present in these cells. We explored these datasets using the functionalities of HitNet and Omics-mod. First, a monotherapy drug screen (BT-40_V1_DS1, referred to as BT-40 except in conjunction with other replicate screens) was conducted for the human low grade glioma cell line model, which harbors a BRAF (proto-oncogene B-Raf) V600E mutation and CDKN2A (Cyclin Dependent Kinase Inhibitor 2A) deletion [46,70]. BT-40 cells were screened as 3D spheroids in a round-bottom 384-well plate against a drug library of 76 (73.5% FDA/EMA approved) drugs, each in 5 concentrations and ATP-based cell viability was detected by CellTiterGlo2.0 assay. The measured drug profiling raw data [Supplementary Table 4]

were analyzed using the QCN and MRA-mod, where the $sDSS_{asym}$ was calculated using the mean DSS_{asym} values obtained from the same drug profiling on a healthy (reference) sample consisting of 5 pediatric healthy control cell samples (astrocytes and peripheral blood mononuclear cells – PBMCs) [Supplementary Table 10]. The output of the MRA-mod analysis indicates a selective sensitivity of several therapies on the BT40 tumor cell line compared to the healthy (reference) samples as shown in the waterfall plot in [Supplementary Fig. 2b], indicated by blue bars for a positive $sDSS_{asym}$ metric while red negative bars represent a negative $sDSS_{asym}$ where the healthy (reference) samples show a higher sensitivity over the BT-40 cells. A full tabulated spreadsheet of the MRA-mod output of the BT-40 cell screen can be downloaded and explored with the drug scores and dose response curves [Supplementary Table 8].

In order to visualize the drug interaction networks using the HitNet module, the drug target genes were annotated to the 76 drug library using the DrugBank database (v.5.1.8) [71], and uploaded to the HitNet-mod. The module features an interactive slider bar to enable the user to adjust the number of drugs that should be included in the network visualization. The number of drug hits can be selected based on the DSS_{asym} or $sDSS_{asym}$ (MRA output). For the BT-40 cells the minimum required number of hits (threshold) to capture drug-drug interactions was four [Supplementary Table 8]. The Omics-mod performs a similar visualization of the drug interactions network with an extra layer of color mapping for the molecular features of the sample (if available) on top of the drug-drug interaction network. This was performed for the BT-40 cells by uploading a tabulated spreadsheet including the molecular features of the cells. The molecular features were uploaded as HUGO symbols of gene fusions, highly expressed genes, single nucleotide variant mutations (SNVs), and gene insertions and deletions (INDELs) [Supplementary Table 11]. The Omics-mod output revealed several mutational events occurring within the drug target interaction network, with a match between both selective BRAF V600E inhibitors included in the library (Dabrafenib) and BRAF single nucleotide variant mutation [Fig. 6a]. Furthermore, the BT-40 cell also showed selectivity towards the second BRAF inhibitor included in the library (Vemurafenib) with an $sDSS_{asym}$ value of (12.3). The second screen with the same 76 drug library was performed for a sarcoma cell line [Supplementary Table 12], established from a pediatric soft tissue sarcoma patient, previously enrolled in the INFORM registry study (INF_R_153_V1_DS1 cell line), and harboring an ETV6-NTRK3-fusion (ETS Variant Transcription Factor 6 - Neurotrophic Receptor Tyrosine Kinase 3) fusion. The screen was analyzed using QCN-mod and MRA-mod similar to the BT-40 cells, the MRA-mod tabulated output [Supplementary Table 13] and $sDSS_{asym}$ waterfall plots [Supplementary Fig. 5a] were explored as described above. The molecular features of the INF_R_153 cell line sample [Supplementary Table 14] were uploaded to Omics-mod. Seven drugs with the highest $sDSS_{asym}$ scores were chosen as threshold to generate an interaction network featuring the NTRK3-fusion. The Omics-mod identified a match between the NTRK inhibitor (Larotrectinib) and the NTRK3 fusion included in the uploaded molecular features of the INF_R_153 cell model. Moreover, Ponatinib was indicated among the selective hit compounds for the INF_R_153 cell line within the MRA mode as indicated by $sDSS_{asym}$ metric of 15.9, which is close to the sensitivity score of Larotrectinib (16.2) [Supplementary Fig. 5b, c]. The Omics-mod identified several other highly expressed biomarkers (GNAI2, GNAI3, CSK, and EPHB2) beside the driver NTRK3 fusion, which may explain the link to the sensitivity to Ponatinib for this particular sample. Ponatinib is an orally active multi-TKI, targeting also ABL; SRC and KIT, which was highly expressed in our soft tissue sarcoma cell model based on RNA sequencing data and act upstream of the identified expressed biomarkers [Fig. 6b].

The MRA-mod output results for the sensitivity of the 76 drug library used to screen both cell line models, BT-40 and INF_R_153, and their

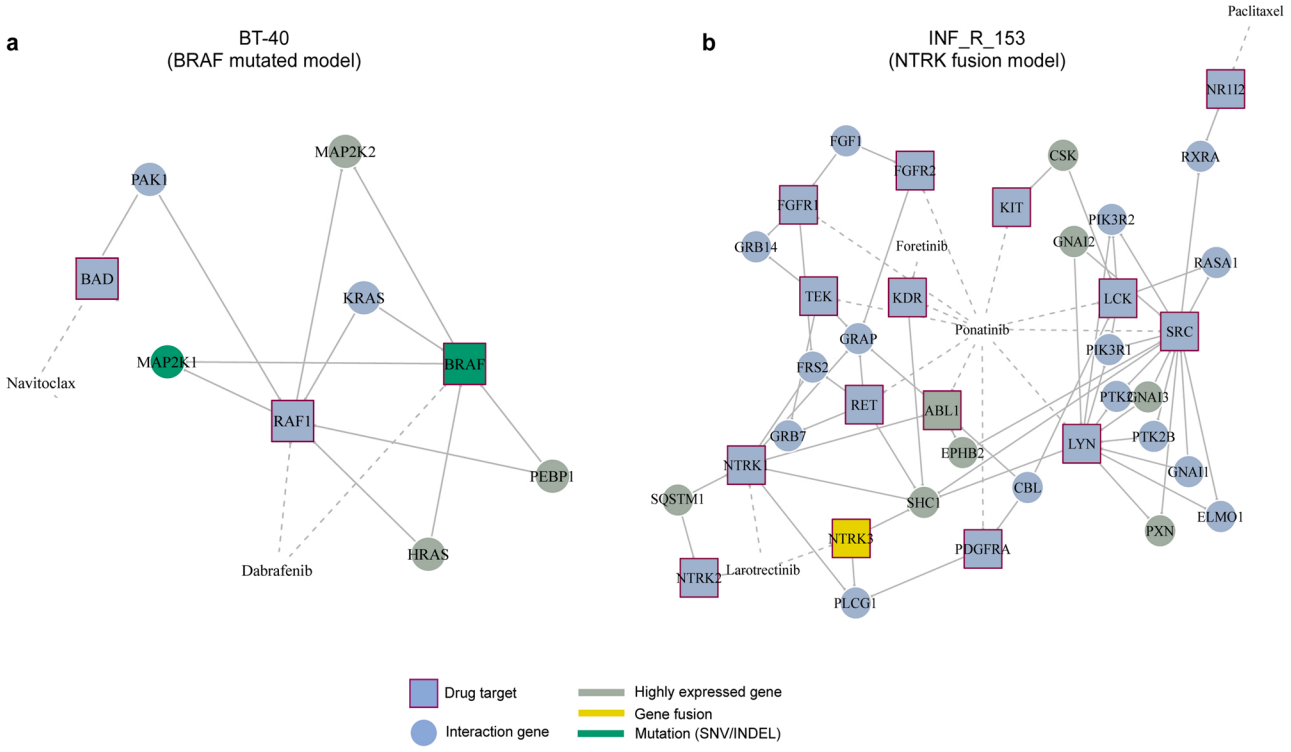

Fig. 6. $sDSS_{asym}$ Drug target interaction network maps using the Omics module. (a) BT-40 model top drug target interaction map (threshold = 4) using the Omics-mod, where squares are drug targets annotated using DrugBank (v5.1.8) and circles are gene biomarker signaling interactions. Different genetic molecular events are distinctly colored, green nodes represent gene variant mutations; olive green nodes represent highly expressed genes. **(b)** INF_R_153 cell line model top drug target interaction map (threshold = 7) using Omics-mod, where the yellow nodes characterize gene fusions, drug targets were annotated using DrugBank (v5.1.8).

biological replicates were used to explore the selectivity of the predicted activity of the BRAF inhibitors and NTRK inhibitors. The $sDSS_{asym}$ metric was used to visualize the selectivity of the therapies in a heatmap [Supplementary Fig. 6], where the NTRK inhibitors (Larotrectinib and Entrectinib) were selectively sensitive to both cell replicates harboring the NTRK3 fusion (INF_R_153_V1_DS1 and INF_R_153_V2_DS1). Moreover, the heatmap revealed the selectivity of the BRAF inhibitors (Vemurafenib and Dabrafenib) on cells harboring the BRAF mutation (BT-40_V1_DS1 and BT-40_V3_DS1). Both cell line models serve as a negative control for each other as indicated in the annotated alterations per cell line [Supplementary Fig. 6]. The heatmap includes further annotation of the expression levels of the potential biomarkers that may explain the interaction between Larotrectinib and Ponatinib, as indicated in the Omics-mod [Fig. 6b], where the EPHB2 biomarker was selectively expressed in the NTRK3 model.

4. Discussion

The field of therapy response profiling is evolving rapidly in both the experimental and computational methods [72,73]. However, it remains challenging for researchers without a bioinformatics background to explore and analyze therapy response profiles with the latest algorithmic developments. It is thus beneficial to have a non-programming application with a graphical user interface that includes state-of-the-art algorithms as routine procedures in the hands of the bench scientists who generate therapy response profiling data. Hence, iTReX, our interactive Shiny web-based application, was developed and designed to analyze and explore mono- and combination therapy dose-response data. The comprehensive application provides a complete workflow including five modules with an intuitive graphical user interface aiming to cover both mono- and combination therapy profiling analysis and to visualize drug target interaction networks and map omics features to the network. iTReX includes an asymmetric drug sensitivity score, motivated by our validation results showing the prevalence of the asymmetric sigmoidal behavior of dose-response curves among various public drug screening datasets [39–42]. The asymmetric DSS is calculated by integrating the drug response after normalization to positive and negative controls and fitting an asymmetric five-parameter curve model. We show that iTReX can further identify the enhanced effects of drug combinations and reproduce synergy findings from earlier published synergy data set [64] using the CRA-mod, which integrates the differential combination asymmetric DSS calculation. This enables the minimal-input experimental set-up, which is ideally developed for preclinical combination studies for PDCs [24,74] or for the first investigational screen for novel drug combinations or drug repositioning opportunities.

Unlike previously developed interactive web-based applications [25–28], iTReX includes the advanced asymmetric fitting approach and surpasses other platforms by including the analysis of combination therapies. Other applications such as SynToxProfiler [30] and SynergyFinder [31] were developed to analyze combination synergy matrix screens only while lacking the monotherapy exploration. In addition, none of the previously developed platforms enable the visualization of drug target interactions and mapping the omics molecular features to the network after processing the therapy response raw data. Using iTReX, omics profiles of any screened models such as patient-derived primary samples can be integrated to construct a drug-target interaction network. The constructed interaction maps show the power of matching drug hits to potential biomarkers and molecular targets for further exploration e.g., in clinical trials. This approach can also be used to construct interaction connectivity networks between top hit enhanced drug combinations, leading to a better understanding of interaction mechanisms of combinations in individual samples. The module can further capture matches between molecular features of a respective sample, i.e., cell line or patient derived sample, to their respective high drug sensitivity targets.

To guide the user through the processing and interpretation of the generated raw data, a step-by-step user manual is provided within the iTReX application for download. This supports the user in data and layout preparation as well as data exploration and interpretation of results and provides data demonstration files, providing the user with an idea what to expect for the iTReX analysis output. Importantly, as data output and results highly depend not only on sample behavior, screening and/or drug/therapy quality, we recommend to first investigate the quality control output and proceed only with the analysis for screens with a good QC, judged by the QC metrics, plate overview for possible edge effects and therapy control behavior if applicable. Moreover, for interpretation of a combinatorial therapy response output (CRA) we recommend to consider all three indicators, the differential combination asymmetric Drug Sensitivity Score ($dcDSS_{asym}$), the percentage inhibition (dPI) per dose as well as the dose response curves of combo and monotherapy. In rare cases the synergy and antagonism curve shift may be influenced by the curve fitting with a false interpretation. Thus, the dPI values are essential to confirm the results of the $dcDSS_{asym}$ metric. A positive $dcDSS_{asym}$ and positive dPI values indicate a synergistic effect, while a negative $dcDSS_{asym}$ confirmed by negative dPI values indicate an antagonistic effect. Additive effects are indicated by overlapping dose response curve of the mono- and combo therapy with dcDSS and dPI near zero. Identified hits could be further validated in extended matrix screens with multiple concentrations per combination partner.

In the future, we will enrich iTReX modules to include additional analysis and visualization capacities. For instance, we will further implement the possibility for testing multiple concentrations of a combination partner added to the concentration range of a library drug and will furtherly work on implementing improvements based on users requests which can be raised through the contact information within the application. The iTReX MRA-mod can be further upgraded by including the computation of the normalized growth rate inhibition method (GRmetrics) [27] that addresses the limitation of cell proliferation rates and the variability of drug concentration ranges applied. The Omics-mod can also integrate correlation and statistical analysis of omics data to the therapy profiling results. We will update iTReX to the newest developments of therapy profiling algorithms and improve the tool to benefit bench scientists towards precision medicine.

5. Conclusion

iTReX allows users to explore drug screening results using interactive visualizations in a sample-specific manner. Moreover, project cohorts analyzed with the MRA and CRA modules can be visualized in a comparative heatmap. Accordingly, both modules enable the exploration of data clusters and thus can be used for hypothesis generation for preclinical and clinical studies. The HitNet and Omics module example cases show how iTReX can advance our views of the biological questions under investigation. Results can support the identification of sample-specific druggable biomarkers and do not only foster individual treatment decisions but also support hypothesis-driven clinical trial designs. iTReX can also act as a personalized exploratory analysis hub for mono- and combination therapy from different screening methods and experimental settings. It is expected that a wide range of users, such as biologists, chemists, pharmaceutical and medical researchers or pharmaceutical companies exploring therapy response data, will benefit from the web application, especially in the area of personalized medicine, where functional treatment profiling is used as a complementary approach to genomic profiling.

Declarations

Ethics approval and consent to participate

For material obtained from patients included in the INFORM study, ethics approval was obtained by the Ethics Committee (EC) of the

Medical Faculty, University of Heidelberg (reference number S-502/2013). Details of the INFORM study including Ethics Commitee approval and patient consent is described by Pfaff et al. [47].

Patients' and parents' written informed consents (Informed Consent Forms (ICFs)) were obtained prior to submission and use of tumor tissue in this study. This includes use of subjects' tumor tissue for research purposes including drug sensitivity profiling and molecular analysis.

The animal PDX experiment performed was conducted in compliance with the national regulations and approved by the Regierungspräsidium Karlsruhe.

Consent for publication

Consent to publish and to report individual patient data has been obtained from patients and parents and is covered through the written informed consents (ICFs) as described in the ethics approval and consent to participate section.

Code availability

The iTReX application is available as a Shiny-based GUI suitable for non-R users at https://itrex.kitz-heidelberg.de. Code is available at http://github.com/the iTReX-Shiny/iTReX.

Funding

This study was supported in parts by funding obtained for the COMPASS project (Clinical implementation Of Multidimensional PhenotypicAl drug SenSitivities in pediatric precision oncology). COMPASS is funded by the Federal Ministry of Education and Research (BMBF) (grant 01KU1903) for DKFZ and Academy of Finland (grant 326249) for FIMM under the frame of ERA PerMed (ERAPERMED2018-121). This work has been supported by SFB 1389-UNITE Glioblastoma, Work Package A02 (OW) and D02 (DH, MS). IO has received funding by the German Cancer Aid, grant 70113843. The study was further supported in part by Kirstins Weg – Verein zur Förderung der Krebsmedizin e.V., and by the Kirstin Diehl-Stiftung (SO, OW).

This work is part of the INFORM registry study (German Clinical Trials Register ID: DRKS00007623), funded by the German Cancer Consortium (DKTK), the German Cancer Aid (DKH), the German Childhood Cancer Foundation (DKS), the German Cancer Research Center (DKFZ) and "Ein Herz für Kinder".

Author's contributions

DE: implemented the Shiny application, conducted bioinformatics analysis, and drafted the manuscript. YB: contributed to code improvement, implementation and testing of the Shiny application. HP: resourced and drafted laboratory methods of cell cultures. IO, VP: supervised laboratory methods of cell cultures. VP, SO: drafted laboratory methods of drug screening and contributed to drug plate layout design and laboratory methods of cell cultures. LT: drafted drug plate layouts, resourced and prepared drug solutions and their dispensing and managed plate shipments. YB, HP, IO, NJ, SO, MS: contributed to software testing. AG: processed the Whole Exome Sequencing (WES) no control workflow. SK, SH: resourced and established the PDX model. NJ, MS: assisted and supervised Omics analysis. OW, MS, SO: provided financial support. SO, MS: conceived the Shiny application and contributed to development, supervised the study and drafted the manuscript. All authors read, commented and approved the final version of the manuscript.

Declaration of Competing Interest

The authors declare that they have no known competing financial interests or personal relationships that could have appeared to influence the work reported in this paper.

Availability of data and materials

The pharmacogenomic raw data of the GDSC, FIMM, gCSI, and GRAY datasets can be directly accessed from the PharmacoGx package [26].

The O'Neil et al. [64], 2016 Merck dataset was obtained by downloading the Supplemental data files associated with O'Neil et al.

The calculated Bliss independent synergy scores and HAS values for the O'Neil data set were downloaded from the DrugComb portal [32], using the following web link: https://drugcomb.fimm.fi.

Tabulated data inputs for the PDX combination screen, and the BT-40 human established cell lines are available on https://github.com/iTReX-Shiny/iTReX Further raw data of human established cell lines and the healthy (reference) sample repository can be obtained upon reasonable request from the authors.

Acknowledgments

We would like to thank Peter J. Houghton (UT Health, San Antonio, Texas) for providing the BT-40 cell line, and Prof. Ewa Koscielniak (Klinikum Stuttgart, Germany) for providing the INF_R_153 cell line. Cancer Society of Finland, Academy of Finland, and Aamu foundation are acknowledged for further funding obtained for VP. Furthermore, we thank the High Throughput Biomedicine core unit of Biocenter Finland (FIMM, HiLIFE, University of Helsinki, Finland), particularly Jani Saarela and Swapnil Potdar for their expertise on assay design and analysis discussions. We thank Olli Kallioniemi for collaboration and hosting a laboratory visit of S.O. and H.P. (FIMM, HiLIFE, University of Helsinki, Finland). We thank Piia Mikkonen, Clarissa Holitsch, Aileen Mangang for their support in the laboratory work of the *ex vivo* cell culture and drug screening. We also thank Rolf Kabbe and Michael Hain for their IT assistance and support deploying the app. Finally, we thank the High Throughput Sequencing unit of the DKFZ Genomics and Proteomics Core Facility for providing the next generation sequencing service and the Omics IT and Data Management Core Facility (ODCF) for the alignment of the Whole Exome Sequencing (WES) data and processing the RNAseq workflow.

Appendix A. Supporting information

Supplementary data associated with this article can be found in the online version at doi:10.1016/j.phrs.2021.105996.

References

[1] J.G. Moffat, F. Vincent, J.A. Lee, J. Eder, M. Prunotto, Opportunities and challenges in phenotypic drug discovery: an industry perspective, Nat. Rev. Drug Discov. 16 (8) (2017) 531–543, https://doi.org/10.1038/nrd.2017.111.

[2] B. Yadav, T. Pemovska, A. Szwajda, E. Kulesskiy, M. Kontro, R. Karjalainen, M. M. Majumder, D. Malani, A. Murumägi, J. Knowles, K. Porkka, C. Heckman, O. Kallioniemi, K. Wennerberg, T. Aittokallio, Quantitative scoring of differential drug sensitivity for individually optimized anticancer therapies, Sci. Rep. 4 (2014) 5193, https://doi.org/10.1038/srep05193.

[3] B. Snijder, G.I. Vladimer, N. Krall, K. Miura, A.S. Schmolke, C. Kornauth, O. Lopez de la Fuente, H.S. Choi, E. van der Kouwe, S. Gültekin, L. Kazianka, J. W. Bigenzahn, G. Hoermann, N. Prutsch, O. Merkel, A. Ringler, M. Sabler, G. Jeryczynski, M.E. Mayerhoefer, I. Simonitsch-Klupp, K. Ocko, F. Felberbauer, L. Müllauer, G.W. Prager, B. Korkmaz, L. Kenner, W.R. Sperr, R. Kralovics, H. Gisslinger, P. Valent, S. Kubicek, U. Jäger, P.B. Staber, G. Superti-Furga, Image-based ex-vivo drug screening for patients with aggressive haematological malignancies: interim results from a single-arm, open-label, pilot study, Lancet Haematol. 4 (2017) e595–e606, https://doi.org/10.1016/S2352-3026(17)30208-9.

[4] T. Mosmann, Rapid colorimetric assay for cellular growth and cytotoxicity assays, J. Immunol. Methods 65 (1983) 55–63.

[5] S. Lindström, Flow cytometry and microscopy as means of studying single cells: a short introductional overview, Methods Mol. Biol. (2012) 13–15, https://doi.org/10.1007/978-1-61779-567-1_2.

[6] B. Haibe-Kains, N. El-Hachem, N.J. Birkbak, A.C. Jin, A.H. Beck, H.J. Aerts, J. Quackenbush, Inconsistency in large pharmacogenomic studies, Nature 504 (7480) (2013) 389–393, https://doi.org/10.1038/nature12831.

[7] M.J. Healy, Statistical analysis of radioimmunoassay data, Biochem. J. 130 (1972) 207–210, https://doi.org/10.1042/bj1300207.

[8] A. Volund, Application of the four-parameter logistic model to bioassay: comparison with slope ratio and parallel line models, Biometrics 34 (1978) 357, https://doi.org/10.2307/2530598.

[9] H. Prinz, Hill coefficients, dose-response curves and allosteric mechanisms, J. Chem. Biol. 3 (2010) 37–44, https://doi.org/10.1007/s12154-009-0029-3.

[10] S.Z. Knezevic, J.C. Streibig, C. Ritz, Utilizing R software package for dose-response studies: the concept and data analysis, Weed Technol. 21 (2007) 840–848, https://doi.org/10.1614/wt-06-161.1.

[11] P.G. Gottschalk, J.R. Dunn, The five-parameter logistic: a characterization and comparison with the four-parameter logistic, Anal. Biochem. 343 (1) (2005) 54–65, https://doi.org/10.1016/j.ab.2005.04.035.

[12] C. Ritz, S.M. Jensen, D. Gerhard, and J.C. Streibig, Dose-Response Analysis Using R, Dose-Response Analysis Using R. 2019. doi: 10.1201/b21966.

[13] F. Commo and Briant M. Bot, "r package n parmater logitic regression," 2016.

[14] J. Ma, E. Bair, A. Motsinger-Reif, Nonlinear dose–response modeling of high-throughput screening data using an evolutionary algorithm, Dose-Response 18 (2) (2020), 1559325820926734, https://doi.org/10.1177/1559325820926734.

[15] M. Fallahi-Sichani, S. Honarnejad, L.M. Heiser, J.W. Gray, P.K. Sorger, Metrics other than potency reveal systematic variation in responses to cancer drugs, Nat. Chem. Biol. 9 (11) (2013) 708–714, https://doi.org/10.1038/nchembio.1337.

[16] T. Pemovska, M. Kontro, B. Yadav, H. Edgren, S. Eldfors, A. Szwajda, H. Almusa, M. M. Bespalov, P. Ellonen, E. Elonen, B.T. Gjertsen, R. Karjalainen, E. Kulesskiy, S. Lagström, A. Lehto, M. Lepistö, T. Lundán, M.M. Majumder, J.M. Marti, P. Mattila, A. Murumägi, S. Mustjoki, A. Palva, A. Parsons, T. Pirttinen, M. E. Rämet, M. Suvela, L. Turunen, I. Västrik, M. Wolf, J. Knowles, T. Aittokallio, C. A. Heckman, K. Porkka, O. Kallioniemi, K. Wennerberg, Individualized systems medicine strategy to tailor treatments for patients with chemorefractory acute myeloid leukemia, Cancer Discov. 3 (12) (2013) 1416–1429, https://doi.org/10.1158/2159-8290.CD-13-0350.

[17] A. Gupta, P. Gautam, K. Wennerberg, T. Aittokallio, A normalized drug response metric improves accuracy and consistency of anticancer drug sensitivity quantification in cell-based screening, Commun. Biol. 3 (1) (2020) 42, https://doi.org/10.1038/s42003-020-0765-z.

[18] J. Barretina, G. Caponigro, N. Stransky, K. Venkatesan, A.A. Margolin, S. Kim, C. J. Wilson, J. Lehár, G.V. Kryukov, D. Sonkin, A. Reddy, M. Liu, L. Murray, M. F. Berger, J.E. Monahan, P. Morais, J. Meltzer, A. Korejwa, J. Jané-Valbuena, F. A. Mapa, J. Thibault, E. Bric-Furlong, P. Raman, A. Shipway, I.H. Engels, J. Cheng, G.K. Yu, J. Yu, P. Aspesi, M. de Silva, K. Jagtap, M.D. Jones, L. Wang, C. Hatton, E. Palescandolo, S. Gupta, S. Mahan, C. Sougnez, R.C. Onofrio, T. Liefeld, L. MacConaill, W. Winckler, M. Reich, N. Li, J.P. Mesirov, S.B. Gabriel, G. Getz, K. Ardlie, V. Chan, V.E. Myer, B.L. Weber, J. Porter, M. Warmuth, P. Finan, J. L. Harris, M. Meyerson, T.R. Golub, M.P. Morrissey, W.R. Sellers, R. Schlegel, L. A. Garraway, The cancer cell line encyclopedia enables predictive modelling of anticancer drug sensitivity, Nature 483 (7391) (2012) 603–607, https://doi.org/10.1038/nature11003.

[19] B. Yadav, T. Pemovska, A. Szwajda, E. Kulesskiy, M. Kontro, R. Karjalainen, M. M. Majumder, D. Malani, A. Murumägi, J. Knowles, K. Porkka, C. Heckman, O. Kallioniemi, K. Wennerberg, T. Aittokallio, Quantitative scoring of differential drug sensitivity for individually optimized anticancer therapies, Sci. Rep. 4 (2014) 5193, https://doi.org/10.1038/srep05193.

[20] A.C. Palmer, C. Chidley, P.K. Sorger, A curative combination cancer therapy achieves high fractional cell killing through low cross resistance and drug Additivity, eLife 8 (2019), https://doi.org/10.7554/eLife.50036.

[21] L. He, E. Kulesskiy, J. Saarela, L. Turunen, K. Wennerberg, T. Aittokallio, J. Tang, Methods for high-throughput drug combination screening and synergy scoring, Methods Mol. Biol. 1711 (2018) 351–398, https://doi.org/10.1007/978-1-4939-7493-1_17.

[22] M. Sinzger, J. Vanhoefer, C. Loos, J. Hasenauer, Comparison of null models for combination drug therapy reveals Hand model as biochemically most plausible, Sci. Rep. 9 (2019) 3002, https://doi.org/10.1038/s41598-019-38907-x.

[23] T. Pemovska, J.W. Bigenzahn, G. Superti-Furga, Recent advances in combinatorial drug screening and synergy scoring, Curr. Opin. Pharmacol. 42 (2018) 102–110, https://doi.org/10.1016/j.coph.2018.07.008.

[24] S. Oppermann, J. Ylanko, Y. Shi, S. Hariharan, C.C. Oakes, P.M. Brauer, J. C. Zúñiga-Pflücker, B. Leber, D.E. Spaner, D.W. Andrews, High-content screening identifies kinase inhibitors that overcome venetoclax resistance in activated CLL cells, Blood 128 (7) (2016) 934–947, https://doi.org/10.1182/blood-2015-12-687814.

[25] O. Pelz, M. Gilsdorf, M. Boutros, Web cellHTS2: a web-application for the analysis of high-throughput screening data, BMC Bioinform. 11 (2010) 185, https://doi.org/10.1186/1471-2105-11-185.

[26] P. Smirnov, Z. Safikhani, N. El-Hachem, D. Wang, A. She, C. Olsen, M. Freeman, H. Selby, D.M. Gendoo, P. Grossmann, A.H. Beck, H.J. Aerts, M. Lupien, A. Goldenberg, B. Haibe-Kains, PharmacoGx: an R package for analysis of large pharmacogenomic datasets, Bioinformatics 32 (8) (2016) 1244–1246, https://doi.org/10.1093/bioinformatics/btv723.

[27] N.A. Clark, M. Hafner, M. Kouril, E.H. Williams, J.L. Muhlich, M. Pilarczyk, M. Niepel, P.K. Sorger, M. Medvedovic, GRcalculator: an online tool for calculating and mining dose-response data, BMC Cancer 17 (1) (2017) 698, https://doi.org/10.1186/s12885-017-3689-3.

[28] S. Potdar, A. Ianevski, J.P. Mpindi, D. Bychkov, C. Fiere, P. Ianevski, B. Yadav, K. Wennerberg, T. Aittokallio, O. Kallioniemi, J. Saarela, P. Östling, Breeze: an integrated quality control and data analysis application for high-throughput drug screening, Bioinformatics 36 (11) (2020) 3602–3604, https://doi.org/10.1093/bioinformatics/btaa138.

[29] A. Malyutina, M.M. Majumder, W. Wang, A. Pessia, C.A. Heckman, J. Tang, Drug combination sensitivity scoring facilitates the discovery of synergistic and efficacious drug combinations in cancer, PLOS Comput. Biol. 15 (2019), 1006752, https://doi.org/10.1371/journal.pcbi.1006752.

[30] A. Ianevski, S. Timonen, A. Kononov, T. Aittokallio, A.K. Giri, SynToxProfiler: an interactive analysis of drug combination synergy, toxicity and efficacy, PLOS Comput. Biol. vol. 16 (2) (2020), e1007604, https://doi.org/10.1371/journal.pcbi.1007604.

[31] A. Ianevski, L. He, T. Aittokallio, J. Tang, SynergyFinder: a web application for analyzing drug combination dose-response matrix data, Bioinformatics 33 (2017) 2413–2415, https://doi.org/10.1093/bioinformatics/btx162.

[32] B. Zagidullin, J. Aldahdooh, S. Zheng, W. Wang, Y. Wang, J. Saad, A. Malyutina, M. Jafari, Z. Tanoli, A. Pessia, J. Tang, DrugComb: an integrative cancer drug combination data portal, Nucleic Acids Res. 47 (2019) 43, https://doi.org/10.1093/nar/gkz337.

[33] A. Kassambara, "ggpubr: 'ggplot2' Based Publication Ready Plots. R package version 0.2.," ⟨https://CRAN.R-project.org/package=ggpubr⟩. 2020.

[34] H. Wickham, R. Francois, L. Henry, and K. Müller, Dplyr: a Grammar of Data Manipulation, 2013. 2017.

[35] H. Wickham, stringr: simple, consistent wrappers for common string operations, R. Package Version (2015).

[36] S. Sauer, "RMarkdown," 2019. doi: 10.1007/978–3-658–21587-3_26.

[37] D. Türei, T. Korcsmáros, J. Saez-Rodriguez, OmniPath: guidelines and gateway for literature-curated signaling pathway resources, Nat. Methods 13 (2016) 966–967, https://doi.org/10.1038/nmeth.4077.

[38] G. Csardi, T. Nepusz, The igraph software package for complex network research, Inter. Complex Syst. (2006).

[39] F. Iorio, T.A. Knijnenburg, D.J. Vis, G.R. Bignell, M.P. Menden, M. Schubert, N. Aben, E. Gonçalves, S. Barthorpe, H. Lightfoot, T. Cokelaer, P. Greninger, E. van Dyk, H. Chang, H. de Silva, H. Heyn, X. Deng, R.K. Egan, Q. Liu, T. Mironenko, X. Mitropoulos, L. Richardson, J. Wang, T. Zhang, S. Moran, S. Sayols, M. Soleimani, D. Tamborero, N. Lopez-Bigas, P. Ross-Macdonald, M. Esteller, N. S. Gray, D.A. Haber, M.R. Stratton, C.H. Benes, L. Wessels, J. Saez-Rodriguez, U. McDermott, M.J. Garnett, A landscape of pharmacogenomic interactions in cancer correspondence resource a landscape of pharmacogenomic interactions in cancer, Cell 166 (2016) 740–754, https://doi.org/10.1016/j.cell.2016.06.017.

[40] J.P. Mpindi, B. Yadav, P. Östling, P. Gautam, D. Malani, A. Murumägi, A. Hirasawa, S. Kangaspeska, K. Wennerberg, O. Kallioniemi, T. Aittokallio, Consistency in drug response profiling, Nature 540 (2016) E5–E6, https://doi.org/10.1038/nature20171.

[41] P.M. Haverty, E. Lin, J. Tan, Y. Yu, B. Lam, S. Lianoglou, R.M. Neve, S. Martin, J. Settleman, R.L. Yauch, R. Bourgon, Reproducible pharmacogenomic profiling of cancer cell line panels, Nature 533 (2016) 333–337, https://doi.org/10.1038/nature17987.

[42] A. Daemen, O.L. Griffith, L.M. Heiser, N.J. Wang, O.M. Enache, Z. Sanborn, F. Pepin, S. Durinck, J.E. Korkola, M. Griffith, J.S. Hur, N. Huh, J. Chung, L. Cope, M.J. Fackler, C. Umbricht, S. Sukumar, P. Seth, V.P. Sukhatme, L.R. Jakkula, Y. Lu, G.B. Mills, R.J. Cho, E.A. Collisson, L.J. van't Veer, P.T. Spellman, J.W. Gray, Modeling precision treatment of breast cancer, Genome Biol. 14 (2013) 110, https://doi.org/10.1186/gb-2013-14-10-r110.

[43] D. Malani, A. Murumägi, B. Yadav, M. Kontro, S. Eldfors, A. Kumar, R. Karjalainen, M.M. Majumder, P. Ojamies, T. Pemovska, K. Wennerberg, C. Heckman, K. Porkka, M. Wolf, T. Aittokallio, O. Kallioniemi, Enhanced sensitivity to glucocorticoids in cytarabine-resistant AML, Leukemia 31 (5) (2017) 1187–1195, https://doi.org/10.1038/leu.2016.314.

[44] C.I. BLISS, The calculation of microbial assays, Bacteriol. Rev. (1956), https://doi.org/10.1128/mmbr.20.4.243-258.1956.

[45] M.C. Berenbaum, What is synergy? Pharmacol. Rev. (1989).

[46] H.K. Bid, A. Kibler, D.A. Phelps, S. Manap, L. Xiao, J. Lin, D. Capper, D. Oswald, B. Geier, M. DeWire, P.D. Smith, R.T. Kurmasheva, X. Mo, S. Fernandez, P. J. Houghton, Development, characterization, and reversal of acquired resistance to the MEK1 inhibitor selumetinib (AZD6244) in an in vivo model of childhood astrocytoma, Clin. Cancer Res. 19 (2013) 6716–6729, https://doi.org/10.1158/1078-0432.CCR-13-0842.

[47] E. Pfaff, A. El Damaty, G.P. Balasubramanian, M. Blattner-Johnson, B.C. Worst, S. Stark, H. Witt, K.W. Pajtler, C.M. van Tilburg, R. Witt, T. Milde, M. Jakobs, P. Fiesel, M.C. Frühwald, P. Hernáiz Driever, U.W. Thomale, M.U. Schuhmann, M. Metzler, K. Bochennek, T. Simon, M. Dürken, M. Karremann, S. Knirsch, M. Ebinger, A.O. von Bueren, T. Pietsch, C. Herold-Mende, D.E. Reuss, K. Kiening, P. Lichter, A. Eggert, C.M. Kramm, S.M. Pfister, D. Jones, H. Bächli, O. Witt, Brainstem biopsy in pediatric diffuse intrinsic pontine glioma in the era of precision medicine: the INFORM study experience, Eur. J. Cancer 114 (2019) 27–35, https://doi.org/10.1016/j.ejca.2019.03.019.

[48] E. Stewart, S.M. Federico, X. Chen, A.A. Shelat, C. Bradley, B. Gordon, A. Karlstrom, N.R. Twarog, M.R. Clay, A. Bahrami, B.B. Freeman, B. Xu, X. Zhou, J. Wu, V. Honnell, M. Ocarz, K. Blankenship, J. Dapper, E.R. Mardis, R.K. Wilson, J. Downing, J. Zhang, J. Easton, A. Pappo, M.A. Dyer, Orthotopic patient-derived xenografts of paediatric solid tumours, Nature 549 (2017) 96–100, https://doi.org/10.1038/nature23647.

[49] E. Reisinger, L. Genthner, J. Kerssemakers, P. Kensche, S. Borufka, A. Jugold, A. Kling, M. Prinz, I. Scholz, G. Zipprich, R. Eils, C. Lawerenz, J. Eils, OTP: An automatized system for managing and processing NGS data, J. Biotechnol. 261 (2017) 53–62, https://doi.org/10.1016/j.jbiotec.2017.08.006.

[50] H. Li, A statistical framework for SNP calling, mutation discovery, association mapping and population genetical parameter estimation from sequencing data, Bioinformatics 27 (2011) 2987–2993, https://doi.org/10.1093/bioinformatics/btr509.
[51] A. Rimmer, H. Phan, I. Mathieson, Z. Iqbal, S. Twigg, A. Wilkie, G. McVean, G. Lunter, Integrating mapping-, assembly- and haplotype-based approaches for calling variants in clinical sequencing applications, Nat. Genet. 46 (2014) 912–918, https://doi.org/10.1038/ng.3036.
[52] J. Jabs, F.M. Zickgraf, J. Park, S. Wagner, X. Jiang, K. Jechow, K. Kleinheinz, U. H. Toprak, M.A. Schneider, M. Meister, S. Spaich, M. Sütterlin, M. Schlesner, A. Trumpp, M. Sprick, R. Eils, C. Conrad, Screening drug effects in patient-derived cancer cells links organoid responses to genome alterations, Mol. Syst. Biol. 13 (11) (2017) 955, https://doi.org/10.15252/msb.20177697.
[53] S. Uhrig, J. Ellermann, T. Walther, P. Burkhardt, M. Fröhlich, B. Hutter, U. H. Toprak, O. Neumann, A. Stenzinger, C. Scholl, S. Fröhling, B. Brors, Accurate and efficient detection of gene fusions from RNA sequencing data, Genome Res. 31 (2021) 448–460, https://doi.org/10.1101/GR.257246.119.
[54] Y. Berker, et al., Patient-by-patient deep transfer learning for drug-response profiling using confocal fluorescence microscopy of pediatric patient-derived tumor-cell spheroids, Manuscript in Revision (2021). Submitted for publication.
[55] X.D. Zhang, A pair of new statistical parameters for quality control in RNA interference high-throughput screening assays, Genomics 89 (2007) 552–561, https://doi.org/10.1016/j.ygeno.2006.12.014.
[56] A. Ianevski, A.K. Giri, P. Gautam, A. Kononov, S. Potdar, J. Saarela, K. Wennerberg, T. Aittokallio, Prediction of drug combination effects with a minimal set of experiments, Nat. Mach. Intell. 1 (2019) 568–577, https://doi.org/10.1038/s42256-019-0122-4.
[57] B.C. Worst, C.M. van Tilburg, G.P. Balasubramanian, P. Fiesel, R. Witt, A. Freitag, M. Boudalil, C. Previti, S. Wolf, S. Schmidt, S. Chotewutmontri, M. Bewerunge-Hudler, M. Schick, M. Schlesner, B. Hutter, L. Taylor, T. Borst, C. Sutter, C. R. Bartram, T. Milde, E. Pfaff, A.E. Kulozik, A. von Stackelberg, R. Meisel, A. Borkhardt, D. Reinhardt, J.H. Klusmann, G. Fleischhack, S. Tippelt, U. Dirksen, H. Jürgens, C.M. Kramm, A.O. von Bueren, F. Westermann, M. Fischer, B. Burkhardt, W. Wößmann, M. Nathrath, S.S. Bielack, M.C. Frühwald, S. Fulda, T. Klingebiel, E. Koscielniak, M. Schwab, R. Tremmel, P.H. Driever, J.H. Schulte, B. Brors, A. von Deimling, P. Lichter, A. Eggert, D. Capper, S.M. Pfister, D.T. Jones, O. Witt, Next-generation personalised medicine for high-risk paediatric cancer patients – the INFORM pilot study, Eur. J. Cancer 65 (2016) 91–101, https://doi.org/10.1016/j.ejca.2016.06.009.
[58] L.M. Packer, S. Rana, R. Hayward, T. O'Hare, C.A. Eide, A. Rebocho, S. Heidorn, M. S. Zabriskie, I. Niculescu-Duvaz, B.J. Druker, C. Springer, R. Marais, Nilotinib and MEK inhibitors induce synthetic lethality through paradoxical activation of RAF in drug-resistant chronic myeloid leukemia, Cancer Cell 20 (2011) 715–727, https://doi.org/10.1016/j.ccr.2011.11.004.
[59] M. Ranzani, K. Kemper, M. Michaut, O. Krijgsman, N. Aben, V. Iyer, K. Wong, T. I. Roumeliotis, M. Velasco-Herrera, J. Nsengimana, G. Turner, N. Thompson, A. Shahrabi, M. Sjoberg, M. Rashid, A.O. Speak, V. Grinkevich, F. Behan, D. Tamborero, F. Iorio, S. van Dongen, G.R. Bignell, C. Alsinet, S. Chen, E. Supper, K. Dutton-Regester, A. Pritchard, C. Wong, A. Enright, J. Newton-Bishop, U. McDermott, N.K. Hayward, J.S. Choudhary, K. Yusa, L. Wessels, M.J. Garnett, D. Peeper, D.J. Adams, A screen for combination therapies in BRAF/NRAS wild type melanoma identifies nilotinib plus MEK inhibitor as a synergistic combination, bioRxiv (2017), https://doi.org/10.1101/195354.
[60] N. Tan, M. Wong, M.A. Nannini, R. Hong, L.B. Lee, S. Price, K. Williams, P.P. Savy, P. Yue, D. Sampath, J. Settleman, W.J. Fairbrother, L.D. Belmont, Bcl-2/Bcl-xL inhibition increases the efficacy of MEK inhibition alone and in combination with PI3 kinase inhibition in lung and pancreatic tumor models, Mol. Cancer Ther. 12 (2013) 853–864, https://doi.org/10.1158/1535-7163.MCT-12-0949.
[61] C. Posch, B.D. Cholewa, I. Vujic, M. Sanlorenzo, J. Ma, S.T. Kim, S. Kleffel, T. Schatton, K. Rappersberger, R. Gutteridge, N. Ahmad, S. Ortiz/Urda, Combined inhibition of MEK and Plk1 has synergistic antitumor activity in NRAS mutant melanoma, J. Investig. Dermatol. 135 (10) (2015) 2475–2483, https://doi.org/10.1038/jid.2015.198.
[62] H.Y. Chen, J. Villanueva, Playing polo-like kinase in NRAS-mutant melanoma, J. Investig. Dermatol. 135 (10) (2015) 2352–2355, https://doi.org/10.1038/jid.2015.253.
[63] H.L. Vu, A.E. Aplin, Targeting mutant NRAS signaling pathways in melanoma, Pharmacol. Res. 107 (2016) 111–116, https://doi.org/10.1016/j.phrs.2016.03.007.
[64] J. O'Neil, Y. Benita, I. Feldman, M. Chenard, B. Roberts, Y. Liu, J. Li, A. Kral, S. Lejnine, A. Loboda, W. Arthur, R. Cristescu, B.B. Haines, C. Winter, T. Zhang, A. Bloecher, S.D. Shumway, An unbiased oncology compound screen to identify novel combination strategies, Mol. Cancer Ther. 15 (2016) 1155–1162, https://doi.org/10.1158/1535-7163.MCT-15-0843.
[65] L. Chaudhuri, N.D. Vincelette, B.D. Koh, R.M. Naylor, K.S. Flatten, K.L. Peterson, A. McNally, I. Gojo, J.E. Karp, R.A. Mesa, L.O. Sproat, J.M. Bogenberger, S. H. Kaufmann, R. Tibes, CHK1 and WEE1 inhibition combine synergistically to enhance therapeutic efficacy in acute myeloid leukemia ex vivo, Haematologica 99 (2014) 688–696, https://doi.org/10.3324/haematol.2013.093187.
[66] S. Hauge, C. Naucke, G. Hasvold, M. Joel, G.E. Rødland, P. Juzenas, T. Stokke, R. G. Syljuåsen, Combined inhibition of Wee1 and Chk1 gives synergistic DNA damage in S-phase due to distinct regulation of CDK activity and CDC45 loading, Oncotarget 8 (2017) 10966–10979, https://doi.org/10.18632/oncotarget.14089.
[67] A. van Erp, L. van Houdt, M. Hillebrandt-Roeffen, N. van Bree, U.E. Flucke, T. Mentzel, J. Shipley, I. Desar, E. Fleuren, Y. Versleijen-Jonkers, W. van der Graaf, Olaparib and temozolomide in desmoplastic small round cell tumors: a promising combination in vitro and in vivo, J. Cancer Res. Clin. Oncol. 146 (2020) 1659–1670, https://doi.org/10.1007/s00432-020-03211-z.
[68] A.F. Farago, B.Y. Yeap, M. Stanzione, Y.P. Hung, R.S. Heist, J.P. Marcoux, J. Zhong, D. Rangachari, D.A. Barbie, S. Phat, D.T. Myers, R. Morris, M. Kem, T.D. Dubash, E. A. Kennedy, S.R. Digumarthy, L.V. Sequist, A.N. Hata, S. Maheswaran, D.A. Haber, M.S. Lawrence, A.T. Shaw, M. Mino-Kenudson, N.J. Dyson, B.J. Drapkin, Combination olaparib and temozolomide in relapsed small-cell lung cancer, Cancer Discov. 9 (2019) 1372–1387, https://doi.org/10.1158/2159-8290.CD-19-0582.
[69] S.J. Gill, J. Travers, I. Pshenichnaya, F.A. Kogera, S. Barthorpe, T. Mironenko, L. Richardson, C.H. Benes, M.R. Stratton, U. McDermott, S.P. Jackson, M. J. Garnett, Combinations of PARP inhibitors with temozolomide drive PARP1 trapping and apoptosis in Ewing's sarcoma, PLOS One 10 (2015), 0140988, https://doi.org/10.1371/journal.pone.0140988.
[70] F. Selt, J. Hohloch, T. Hielscher, F. Sahm, D. Capper, A. Korshunov, D. Usta, S. Brabetz, J. Ridinger, J. Ecker, I. Oehme, J. Gronych, V. Marquardt, D. Pauck, H. Bächli, C.D. Stiles, A. von Deimling, M. Remke, M.U. Schuhmann, S.M. Pfister, T. Brummer, D. Jones, O. Witt, T. Milde, Establishment and application of a novel patient-derived KIAA1549: BRAF-driven pediatric pilocytic astrocytoma model for preclinical drug testing, Oncotarget 8 (2017) 11460–11479, https://doi.org/10.18632/oncotarget.14004.
[71] D.S. Wishart, C. Knox, A.C. Guo, D. Cheng, S. Shrivastava, D. Tzur, B. Gautam, M. Hassanali, DrugBank: a knowledgebase for drugs, drug actions and drug targets, Nucleic Acids Res. 36 (2008) D901–D906, https://doi.org/10.1093/nar/gkm958.
[72] H. Xue, J. Li, H. Xie, Y. Wang, Review of drug repositioning approaches and resources, Int. J. Biol. Sci. 14 (2018) 1232–1244, https://doi.org/10.7150/ijbs.24612.
[73] G. Adam, L. Rampášek, Z. Safikhani, P. Smirnov, B. Haibe-Kains, A. Goldenberg, Machine learning approaches to drug response prediction: challenges and recent progress, npj Precis. Oncol. 4 (2020) 19, https://doi.org/10.1038/s41698-020-0122-1.
[74] M. Shehata, S. Schnabl, D. Demirtas, M. Hilgarth, R. Hubmann, E. Ponath, S. Badrnya, C. Lehner, A. Hoelbl, M. Duechler, A. Gaiger, C. Zielinski, J. D. Schwarzmeier, U. Jaeger, Reconstitution of PTEN activity by CK2 inhibitors and interference with the PI3-K/Akt cascade counteract the antiapoptotic effect of human stromal cells in chronic lymphocytic leukemia, Blood 116 (2010) 2513–2521, https://doi.org/10.1182/blood-2009-10-248054.